NASA TECHNICAL NOTE

NASA TN D-5928

TURBINE AERODYNAMIC AND COOLING REQUIREMENTS FOR A TURBOJET POWERED MACH 3 TRANSPORT USING METHANE FUEL

by David G. Evans, Keith A. Furgalus, and Francis S. Stepka

Lewis Research Center
Cleveland, Ohio 44135

NATIONAL AERONAUTICS AND SPACE ADMINISTRATION • WASHINGTON, D. C. • AUGUST 1970

1. Report No. NASA TN D-5928	2. Government Accession No.	3. Recipient's Catalog No.
4. Title and Subtitle TURBINE AERODYNAMIC AND COOLING REQUIREMENTS FOR A TURBOJET POWERED MACH 3 TRANSPORT USING METHANE FUEL		5. Report Date August 1970 6. Performing Organization Code
7. Author(s) David G. Evans, Keith A. Furgalus, and Francis S. Stepka		8. Performing Organization Report No. E-5602
9. Performing Organization Name and Address Lewis Research Center National Aeronautics and Space Administration Cleveland, Ohio 44135		10. Work Unit No. 720-03 11. Contract or Grant No. 13. Type of Report and Period Covered
12. Sponsoring Agency Name and Address National Aeronautics and Space Administration Washington, D.C. 20546		Technical Note 14. Sponsoring Agency Code

15. Supplementary Notes

16. Abstract

An analysis is presented of two-stage air-cooled turbines designed for a series of afterburning and nonafterburning turbojet engines. The study considers the effects of turbine inlet temperature, takeoff jet noise, blade thermal cooling effectiveness, wall cooling, and precooling of the cooling air on turbine aerodynamic design and cooling airflow requirements. Blade and wall cooling requirements increased rapidly with increasing turbine inlet temperature. As a result, essentially no increase in turbine exit temperature or pressure was possible beyond a turbine inlet temperature of approximately 2500° F (1645 K) for the compressor pressure ratios, turbine metal temperatures, and turbine cooling methods considered.

17. Key Words (Suggested by Author(s)) Turbine design Turbine cooling Turbojet engines Methane-fueled engines Supersonic propulsion systems	18. Distribution Statement Unclassified - unlimited

19. Security Classif. (of this report)	20. Security Classif. (of this page)	21. No. of Pages	22. Price*
Unclassified	Unclassified	80	$3.00

*For sale by the Clearinghouse for Federal Scientific and Technical Information
Springfield, Virginia 22151

CONTENTS

TURBINE AERODYNAMIC AND COOLING REQUIREMENTS FOR A TURBOJET POWERED MACH 3 TRANSPORT USING METHANE FUEL

by David G. Evans, Keith A. Furgalus, and Francis S. Stepka
Lewis Research Center

SUMMARY

The results of an analysis of the turbine aerodynamic and cooling requirements for eight liquid-methane-fueled turbojet engines designed for a 460 000-pound (208 651-kg) Mach 3 transport are presented. Four of the turbines were designed for nonafterburning (dry) turbojet engines ranging in turbine inlet temperature from 2200° to 3100° F (1478 to 1978 K). The remaining four turbines were designed for 2200° F (1478 K) engines which satisfied various afterburning or noise requirements at takeoff.

The study was conducted to obtain comprehensive design information on the aerodynamic, thermodynamic, cooling, and dimensional requirements for the turbines. The analysis began with a three-dimensional development of the velocity diagram requirements for the turbines. From this, the gas stream pressures and temperatures, blade dimensions and heat-transfer coefficients, and cooling airflow ratios required to convectively cool the blades, and to film cool the hub and tip walls, were determined. Turbine cooling air temperature reductions (precooling) of from 0° to 600° F (0 to 333 K) below compressor discharge temperature were considered, indicative of using various amounts of the heat sink of the methane to cool the air.

The results indicated that two-stage turbines adequately met the power and performance requirements of the eight engines, and were aerodynamically and dimensionally conventional in design. Turbine tip diameters varied from 44 to 54 inches (112 to 137 cm), blade heights from 2.5 to 11.2 inches (6.4 to 28.4 cm), and the number of blades per row from 27 to 208.

The total cooling airflow ratios (turbine cooling air to compressor weight flow ratio) varied from 0.064 to 0.070 for the five 2200° F (1478 K) turbines, to 0.13, 0.21, and 0.30 for the 2500°, 2800°, and 3100° F (1645, 1811, and 1978 K) turbines. As a result of the high cooling airflow ratios required for the latter two turbines, no increase in either turbine exit temperature or pressure was possible beyond a turbine inlet temperature of approximately 2500° F (1645 K) for the compressor pressure ratios, turbine metal temperatures, and turbine cooling methods considered.

At a blade thermal cooling effectiveness of 0.50, twice as much cooling air was required to cool the blades as to cool the walls. Increasing the blade thermal cooling effectiveness to 0.70 reduced the amount of blade cooling air by a fourth. Reducing the temperature of the cooling air 400° F (222 K) reduced the total amount of cooling air by 36 to 40 percent.

INTRODUCTION

An analytical investigation was conducted to determine the effects of turbine inlet temperature, takeoff jet noise restrictions, blade thermal cooling effectiveness, and cooling air precooling on the aerodynamic and cooling requirements of air-cooled turbines for methane-fueled afterburning and nonafterburning (dry) turbojet engines designed to power a Mach 3 transport aircraft.

Recent studies of advanced propulsion systems for supersonic transport aircraft have indicated several directions in which future engine technology may go. Three major areas have stimulated particular interest because of their potentially large effect on aircraft and engine size and performance. They are (1) converting from JP-kerosene type fuels to liquid methane; (2) further increases in turbine inlet temperature, and hence engine performance, afforded by the potential use of the high heat-sink of liquid methane fuel to cool the turbine; and (3) reducing engine jet noise during takeoff and initial climb.

In reference 1, an evaluation was made of the relative differences in aircraft performance between using liquid methane and JP-type fuels in a Mach 3, SCAT 15F, 460 000-pound (208 651-kg) gross weight transport. The results indicated that the payload of the liquid-methane-fueled transport could be increased up to 18 percent over the JP-fueled transport primarily because of the higher heating value of methane. It was also indicated that by utilizing the high heat-sink capacity of liquid methane to reduce the temperature of the turbine cooling air, turbine inlet temperatures could be increased substantially beyond current limits, allowing for a further increase in payload to approximately 30 percent over the JP-fueled transport.

A similar analysis (ref. 2) further defined the effects of elevated turbine inlet temperature on payload, and also considered the effect of reductions in takeoff jet noise on the engine design requirements and payload. In the study, only increases in engine weight flow were considered to reduce jet velocities and jet noise while still maintaining an acceptable takeoff distance. The resulting increase in the weight and drag of the propulsion system decreased the payload from 1 to 10 percent, respectively, for the dry and afterburning turbojet engines considered in the study. Also, there was no payload advantage in going to turbine inlet temperatures above 2200° F (1478 K). However, without the noise restrictions imposed on the design of the engine, reference 2 indicated approximately the same trends of increasing payload with increases in turbine inlet temperatures as were noted in reference 1.

In arriving at these conclusions, it was unavoidable that approximations were made in specifying the performance criteria for the engines. A more detailed study of the engine components most affected by a conversion to liquid methane fuel was required. The turbine was one of the first components considered because of the large variation in turbine weight flow, work, and speed necessary to cover the range of engine vari-

ables and engine types considered in references 1 and 2. Realistic turbine design information was also required in support of research efforts investigating the heat-transfer characteristics of turbines and the heat-sink capacity of the fuel for turbine cooling. The necessary information included estimates of the turbine cooling airflow requirements, turbine gas stream temperatures, pressures, and velocities, and turbine blade and hub and tip wall dimensions and surface areas.

In this report, the general dimensional configuration and operating requirements for the turbine are determined in a detailed three-dimensional design study of a series of turbines specifically designed for methane-fueled turbojet-type engines. Four of the turbines analyzed are for the dry turbojet engines considered in reference 2, ranging in turbine inlet temperature from 2200° to 3100° F (1478 and 1978 K). Two additional turbines are analyzed for an afterburning turbojet engine designed to operate at a turbine inlet temperature of 2200° F (1478 K): one sized for maximum afterburning, and the other sized for no afterburning at takeoff. The final designs are of turbines suitable for the dry and afterburning turbojet engines capable of meeting the noise restraints of reference 2. No turbine designs for turbofan-type engines were considered.

Velocity diagrams, inner-stage gas pressures and temperatures, blade annulus dimensions, approximate blade shapes, exposed blade surface areas, and coolant airflow ratios are determined for each of the turbine designs. In determining these requirements, a range of cooling air temperature reductions of from 0° to 600° F (0 to 333 K) below compressor discharge temperature is used, which is assumed herein to be indicative of using various amounts of the heat-sink capacity available in the liquid methane fuel. From this descriptive information, comparisons are then made of the effects of higher turbine inlet temperatures or lower takeoff jet noise on the design and operating requirements of the turbines.

SELECTION OF ENGINES AND TURBINES

The engine specifications evolved from references 1 and 2 for a Mach 3, SCAT 15F, 460 000-pound (208 651-kg) gross weight liquid-methane-fueled transport were used to define the design requirements for the various turbines investigated. Only turbines for nonafterburning (dry) and afterburning turbojet engines were considered, and the specifications for these turbojet engines are given in table I, and in figures 1 and 2. The symbols noted on the figures are defined in appendix A.

The dry turbojet engines, designed as A, B, C, and D in table I, were selected to study the effects that increasing the turbine inlet temperature from 2200° to 3100° F (1478 to 1978 K) would have on the design of the turbines. The remaining engines, designated in table I as E, F, and G were selected to study the effects that changes in the mode of engine operation, brought about by reduced jet noise at takeoff, would have on

TABLE I. - DESIGN SPECIFICATIONS

(a) Engine

Specification	Engine designation						
	A	B	C	D	E	F	G
	Engine type						
	Dry turbojet				Quiet dry or afterburning turbojet	Afterburning turbojet	
Takeoff power,[a] percent	100				86 (Dry)	100 (Dry)	100 (Aug.)
Ratio of thrust to aircraft gross weight at takeoff,[a, b]	0.357	0.359				0.320	
Thrust sizing criteria[a]	Transonic acceleration		Maximum payload		Jet noise and maximum takeoff roll[c]	Maximum takeoff roll[c]	

(b) Aircraft

Payload, number of passengers	230	249	262	270	[d]227 [e]215	239	240
Jet noise at takeoff,[a, b] PNdB	120.8	123.0	124.2	124.6	116.0	120.8	122.3

(c) Turbine

Inlet temperature,[a, f] $T'_{T,1}$, °F (K)	2200 (1478)	2500 (1645)	2800 (1811)	3100 (1978)	2200 (1478) [g]1755 (1230)	2200 (1478)	
Cooling airflow ratio,[a, f] y'	0.06	0.09	0.12	0.15		0.06	
Total efficiency,[h] η	0.90	0.89	0.88	0.87		0.90	

(d) Compressor

Design pressure ratio,[a, i] $(p'_2/p'_1)_C$:							
Takeoff	8.35	11.15	14.75	19.00	8.00 [g](7.44)	10.00	
Cruise	2.98	3.87	4.99	6.40	2.85	3.51	
Design corrected weight flow,[a] $(w\sqrt{\theta}/\delta)_{C,1}$, lb/sec (kg/sec):							
Takeoff	528 (239)	468 (212)	423 (192)	386 (175)	553 (251)	443 (201)	353 (160)
Cruise	272 (124)	242 (110)	212 (96)	192 (87)	285 (129)	226 (103)	180 (82)
Rotational speed,[f] rpm	5580	5920	6235	6520	5460	6100	6825
Tip diameter, $D_{t,C}$, in. (cm)	53.40 (135.6)	50.30 (127.8)	47.80 (121.5)	45.70 (116.1)	54.60 (138.6)	48.88 (124.1)	43.65 (110.9)
Exit temperature at cruise, $T'_{C,2}$, °F (K)	1072 (851)	1190 (917)	1310 (984)	1428 (1049)	1055 (842)	1144 (891)	

(e) Additional component design criteria

Criterion	Takeoff	Mach 3 cruise
Inlet loss total-pressure ratio,[a] $(p'_2/p'_1)_i$	0.950	0.851
Compressor inlet temperature,[a] $T'_{C,1}$, °F (K)	59 (288)	623 (602)
Compressor corrected weight flow per frontal area $\left[(w\sqrt{\theta}/\delta)/A_f\right]_{C,1}$, lb/(sec)(ft^2) (kg/(sec)(m^2))	34.0 (15.42)	[j]
Compressor efficiency,[a] η_C	0.87	0.82
Compressor tip speed, $U_{t,C,1}$, ft/sec (m/sec)	1300 (396)	1300 (396)
Primary burner efficiency,[a] η_B	0.98	0.98
Burner loss total-pressure ratio,[a] $(p'_2/p'_1)_B$	0.94	0.94
Afterburner exit temperature, °F (K)	[k]3100 (1978)	[j, k]

[a] From ref. 1 and or ref. 2.
[b] For four engines.
[c] Maximum takeoff roll, 4450 ft (1356 m).
[d] Dry turbojet engine
[e] Afterburning turbojet engine.
[f] Value at takeoff and cruise.
[g] Value at takeoff when different from design.
[h] Assumed value.
[i] Optimum payload value.
[j] Value varies between engines.
[k] When used.

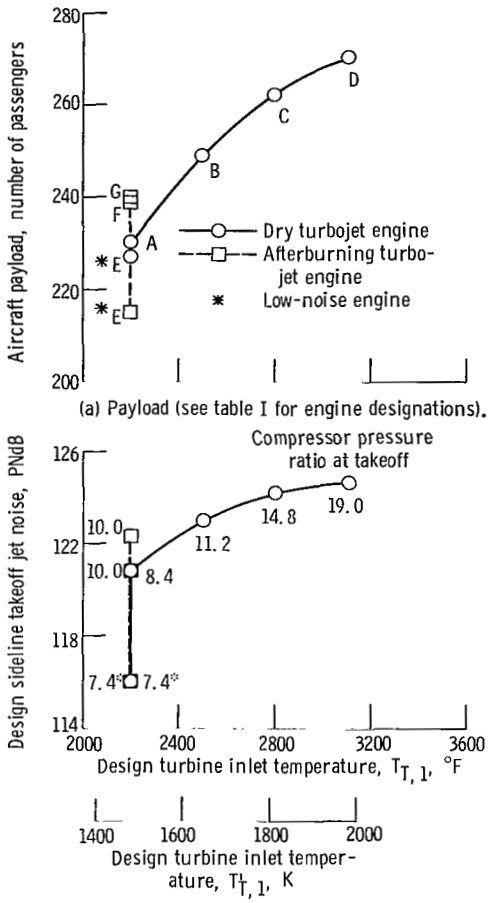

(a) Payload (see table I for engine designations).

(b) Engine noise and pressure ratio.

Figure 1. - Effect of turbine inlet temperature and engine type on aircraft payload, sideline takeoff jet noise, and compressor pressure ratio.

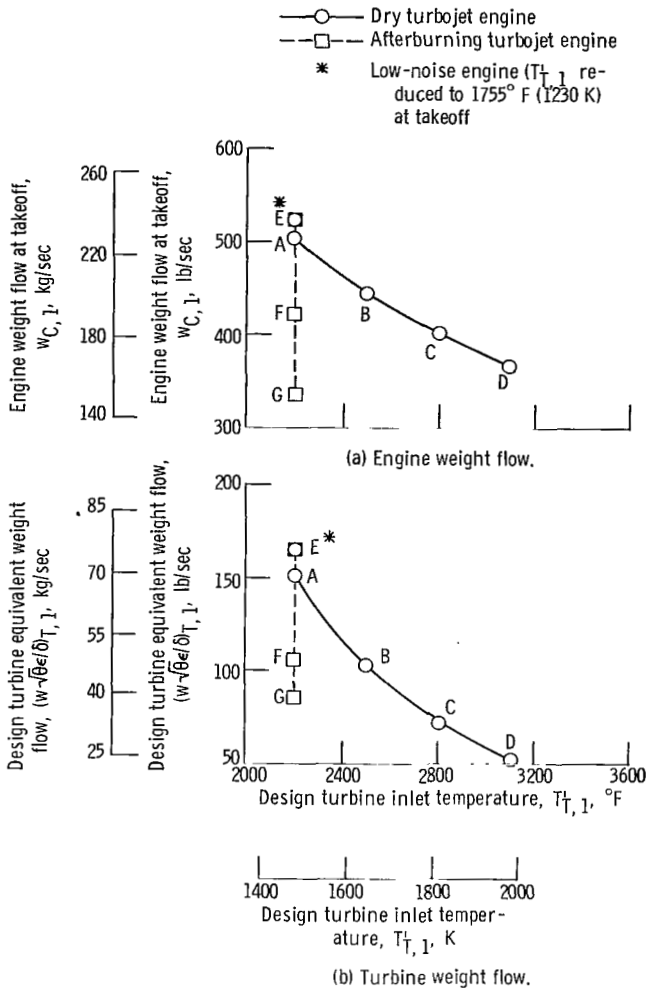

(a) Engine weight flow.

(b) Turbine weight flow.

Figure 2. - Effect of turbine inlet temperature and engine type on weight flow. (See table I for engine designations.)

the design of a 2200° F (1478 K) turbine. Selected were two afterburning turbojet engines sized for maximum afterburning, 3100° F (1978 K), and no afterburning at takeoff to reduce jet noise 1500 feet (457 m) to the side of the airplane to an assumed hypothetical value of 116 PNdB. The thrust sizing criteria used to determine the weight flow for each engine, and the resultant thrust-to-aircraft-gross-weight ratios at takeoff are shown in table I.

The low-noise engine could be either an afterburning or dry turbojet engine since the specifications for both engines, as noted in table I, are identical. The difference is seen only in terms of the payload and, as will be discussed later, in the turbine exit critical velocity ratio used. As noted in the INTRODUCTION, jet noise was reduced by reducing jet velocity. Therefore, an increase in engine size and weight flow was required

to reduce the noise and still meet takeoff distance constraints. This increase is evident in comparing engine weight flows with jet noise in table I. Only engines designed for a turbine inlet temperature of 2200° F (1478 K) were considered for the low-noise engines since the results of reference 2 indicated that there would be little or no payload advantage in going to higher turbine inlet temperatures with the turbojet-type of engine. However, to reduce jet noise to 116 PNdB and not exceed the maximum takeoff roll distance of 4450 feet (1356 m), it was necessary to increase the size and weight flow of the engines, and to decrease the turbine inlet temperature from its design value of 2200° F (1478 K) to a value of 1755° F (1230 K) during takeoff. These changes are evident in comparing engines A, F, and G in table I with engine E.

For illustrative purposes, figure 1 plots these engines in terms of engine type and turbine inlet temperature. Turbine inlet temperature $T'_{T,1}$ is defined as the average total temperature of the gas at the inlet of the first-stage stator. The figure notes the range of payload, sideline jet noise at takeoff, and design compressor pressure ratio at takeoff obtained from the analyses of references 1 and 2 for each engine.

The values of compressor corrected weight flow per compressor frontal area and compressor tip speed given in table I had to be assumed in order to determine compressor tip diameters and engine rotational speeds. Equal rotational speeds were assumed at takeoff and Mach 3 cruise. The value of compressor pressure ratio used for each engine, noted in table I and figure 1(b), was the value found necessary in the analyses of references 1 and 2 to optimize the payload. The turbine cooling airflow ratios (turbine cooling air to compressor weight flow ratio) noted in table I were approximate values used in the analyses of references 1 and 2, and reflect the use of a portion of the heat-sink capacity of the methane fuel to reduce the temperature of the cooling air.

For illustrative purposes, the resulting values of compressor (engine) weight flow are shown in figure 2(a). Also, corresponding values of turbine equivalent weight flow are shown in figure 2(b). Included in the calculation of turbine equivalent weight flow was the primary burner fuel flow minus the turbine cooling airflow extracted at the compressor exit.

TURBINE DESIGN CONSIDERATIONS

The general flow model used in the analysis of the turbines is shown in figure 3. In it, the air required to cool the turbine was extracted at the exit of the compressor and cooled in a fuel-to-air heat exchanger before entering the turbine. Sufficient quantities of fuel were then burned with the remaining compressor exit air to produce the desired turbine inlet temperature of from 2200° to 3100° F (1478 to 1978 K). In this simplified model, the heat sink of the fuel was used to decrease the temperature of the cooling air.

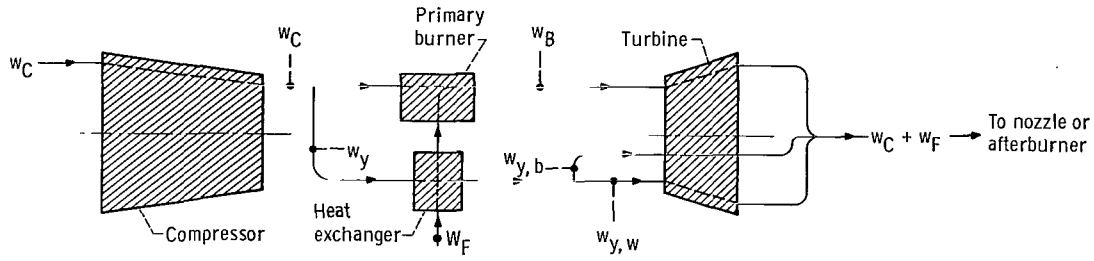

Figure 3. - Engine components and general flow model.

More complex fuel systems, in which the additional heat-sink of ram-air heat exchangers or expansion turbines are included, are discussed in reference 3. For purposes of the present analysis, three cooling air temperature reductions were assumed: 0°, 200°, and 400° F (0, 111, and 222 K), representative of using various amount of the heat sink available within the fuel system. The majority of the analysis was conducted at a cooling air temperature reduction of 400° F (222 K). A fourth value, 600° F (333 K), was also considered for one of the dry turbojet turbines.

Variations in the flow model were devised to assist in analyzing the effects that the cooling air would have on determining the number of stages, specific work, velocity diagrams, temperature drop, and blade height requirements for the eight turbines investigated. These additional models, together with a detailed description of the turbine design procedure are developed in appendixes B to H. Appendixes B, C, and D describe the criterion used for determining the number of stages, specific work, velocity diagram requirements, and gas stream pressures and temperatures. The techniques used to determine turbine blade geometry, blade cooling air requirements, and turbine hub and tip wall cooling air requirements are described in appendixes E, F, and G.

Finally, the method by which the above aerodynamic, thermodynamic, and cooling airflow requirements are combined and incorporated into the final design of the turbines is described in appendix H. Therein, turbine inner-stage temperatures, flow rates, and blade heights are adjusted to include the effects of discharging the cooling air from each blade row and wall into the main gas stream.

Turbines having from one to three stages were considered in the analyses. However, only the design requirements of two-stage turbines were developed. These requirements were determined from a study of the three-dimensional (blade hub, mean, and tip section) velocity diagrams for each turbine at a fixed level of hub reaction across each rotor blade row. The additional assumptions, including those of work-split between stages, stage and overall efficiency, exit leaving angle, and exit critical velocity ratio are noted in appendix D Blade configurations were determined from a series of working curves developed from the dimensional characteristics of the blading used in many present day turbines and engines. Finally, the amount of cooling air required to

cool each turbine was determined by equating the heat sink required to cool each blade and each hub and tip wall to the heat sink available in the cooling air for the select value of cooling air temperature reduction and blade thermal cooling effectiveness used. Average stator blade, rotor blade, and wall metal temperatures of 1720^{o}, 1620^{o}, and 1600^{o} F (1211, 1155, and 1145 K) were used. These temperatures were assumed to be reasonable for a 1000-hour life expectancy based on the appropriate stress-rupture, cyclic, creep, and oxidation properties of currently available alloys and coating.

Because turbine cooling airflow requirements and specific work requirements are generally more critical at high flight Mach numbers than at takeoff, only cruise values of these parameters were determined and used in the design of the turbines. In the analyses of references 1 and 2, the average altitude at the beginning of cruise was found to vary from 70 000 to 72 000 feet (21 350 to 21 950 m) with engine type and turbine inlet temperature. For convenience, a constant value of 70 000 feet (21 350 m) was used herein to determine the cooling airflow requirements. However, because of this variation in cruise altitude between engines, it was found more convenient to use turbine takeoff weight flow rather than cruise weight flow to size the turbines.

RESULTS AND DISCUSSION

A description and comparison is presented in this section of the turbine designs evolved for the eight methane-fueled, Mach 3 transport engines discussed previously. The performance characteristics of turbines having from one to three stages are surveyed in appendix B, and it was determined therein that two-stage turbines were best suited to the range of turbine inlet temperatures and engine types considered in the analysis. Therefore, only the design characteristics of two-stage turbines were investigated.

Four of the designs are of turbines suitable for dry turbojet engines having turbine inlet temperatures of 2200^{o}, 2500^{o}, 2800^{o}, and 3100^{o} F (1478, 1645, 1811, and 1978 K), and are designated as engines A to D in table I. Two of the designs are of turbines suitable for the 2200^{o} F (1478 K) afterburning turbojet engines designated G and F. Engine G was sized for maximum afterburning at takeoff, and engine F was sized for no afterburning at takeoff to reduce jet noise. The last two designs, designated E in table I, are of turbines applicable to both types of engines, but sized to operate at an assumed hypothetical value of 116 PNdB side-line jet noise at takeoff.

A general description of the turbines is presented, followed by a detailed description of their aerodynamic and thermodynamic characteristics, blade geometry, and cooling airflow requirements.

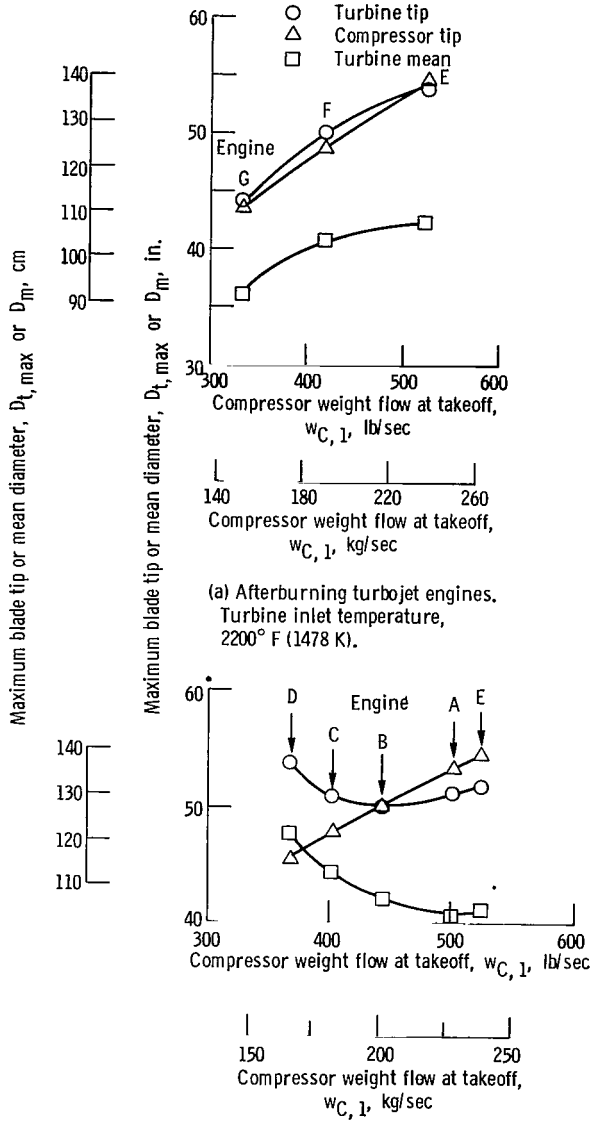

(a) Afterburning turbojet engines. Turbine inlet temperature, 2200° F (1478 K).

(b) Dry turbojet engines.

Figure 4. - Turbine and compressor diameters. Pattern factor, 0.15; blade thermal cooling effectiveness, 0.70; and cooling air temperature reduction across the cooling air heat exchanger, 400° F (222 K). (See table I for engine designations.)

General Description

The salient features of the turbines evolved for the three afterburning and five dry turbojet engines are illustrated in figures 4 and 5, respectively, and tabulated in table II. The turbine parameters noted are the mean blade and tip diameters as a function of compressor weight flow (fig. 4), the turbine cooling airflow ratios as a function of turbine inlet temperature (fig. 5), and the turbine blade heights, turbine blade radius ratios, and turbine axial critical velocity ratios (table II). For comparison, compressor tip diameters are included in figure 4. All values are for a burner pattern factor PF of 0.15, a blade thermal cooling effectiveness Λ of 0.70, and a cooling air temperature reduction across the cooling air heat exchanger $\Delta T'_{HX,y}$ of 400° F (222 K). In addition, comparisons of cooling airflow ratio are shown in figure 6 for values of Λ of 0.70 and 0.50 for a range of $\Delta T'_{HX,y}$ of 0° to 600° F (0 to 333 K) for two of the turbines.

Turbine diameters. - Turbine tip diameters for the three afterburning turbojet engines designated E, F, and G (fig. 4(a)) varied from 44 inches (112 cm) for the small, low-flow noisy engine G designed to afterburn at takeoff, to 54 inches (137 cm) for the large high-flow quiet engine E. The compressor tip diameters, repeated from table I, are also shown for comparison. The turbines were nearly equal in tip diameter to the compressors they were driving.

Whereas the ratio of turbine-to-compressor tip diameter for the two noisy engines F and G was only slightly greater than 1, it was slightly less than 1 for quiet engine E. This reduction in the ratio was due to the generally reduced level of specific work and pressure ratio required for turbine E, as will be shown later, and to the effect this reduction had on turbine mean diameter and exit blade height.

The variation in turbine diameter with compressor weight flow is compared with compressor tip diameter in figure 4(b) for the five dry turbojet engines, designated A to E. Whereas the afterburning turbojet turbines were approximately equal in tip diameter to their respective compressors, the turbines for the dry turbojet engines A and E, having the same turbine inlet temperature of 2200° F (1478 K), were 2 inches (5.1 cm) smaller in diameter. The resulting reduction in the turbine-to-compressor diameter ratio was due to the increase in turbine exit axial critical velocity ratio assumed in the design of the dry turbojet turbines. This increase in exit critical velocity ratio resulted in a reduction in the mean diameter and blade height of the turbines.

At the higher turbine inlet temperatures considered for engines B, C, and D, turbine tip diameters equaled or exceeded the tip diameter of their respective compressors. Turbine diameters increased rapidly beyond a turbine inlet temperature of 2500° F (1645 K) even though compressor weight flows continued to decrease. Between 2500° and 3100° F (1645 and 1978 K), turbine tip diameters increased 8 percent from 50 to 54 inches (127 to 137 cm), while compressor tip diameters decreased 9 percent

TABLE II. - OVERALL TURBINE DESIGN CHARACTERISTICS

Characteristic	Engine designation[a]							
	A	B	C	D	E	E	F	G
	Engine type							
	Dry turbojet					Afterburning turbojet		
Design turbine inlet temperature, $T'_{T,1}$, ^{o}F (K)	2200 (1478)	2500 (1645)	2800 (1811)	3100 (1978)		2200 (1478)		
Turbine blade height, BH, in. (cm):								
Inlet, first stage	9.02 (22.92)	6.04 (15.35)	3.99 (10.14)	2.54 (6.45)	10.03 (25.48)	8.63 (21.92)	6.27 (15.93)	5.49 (13.95)
Exit, second stage	10.26 (26.08)	8.10 (20.59)	6.68 (16.97)	6.21 (15.78)	10.64 (27.01)	11.21 (28.48)	9.51 (24.16)	8.08 (20.52)
Turbine blade radius ratio, r_h/r_t:								
Inlet, first stage	0.64	0.75	0.83	0.90	0.61	0.66	0.73	0.74
Exit, second stage	.60	.68	.74	.77	.59	.58	.62	.63
Turbine axial critical velocity at cruise, V_x/V_{cr}:								
Inlet, first stage	0.24	0.25	0.23	0.23	0.24	0.28	0.25	0.26
Inlet, second stage	.36	.38	.38	.38	.36	.39	.37	.37
Exit, second stage (station 2)	.50	.51	.52	.52	.51	.45	.43	.45

[a]See table I for details.

from 50 to 46 inches (127 to 117 cm). Therefore, at the peak turbine inlet temperature investigated of 3100° F (1978 K), the turbine was 8 inches (20 cm) larger in diameter than its compressor. The increase in the turbine-to-compressor diameter ratio was due to the considerable increase in turbine specific work with increasing turbine inlet temperatures, as will be shown later, and to the effect this increase in turbine specific work had on increasing the turbine mean diameter.

Turbine blade heights and radius ratios. - Turbine blade heights for the three afterburning turbojet turbines G, F, and E varied from 5.49 to 8.63 inches (13.95 to 21.92 cm) at the turbine inlet, and from 8.08 to 11.21 inches (20.52 to 28.48 cm), respectively, at the turbine exit. This variation in blade height is shown in table II and, as will be noted later, in figure 14. The corresponding values of blade radius ratio are also shown in the table, and varied from approximately 0.735 at the inlet of the two turbines designed for the noisy engines F and G, to 0.66 for the turbine designed for the quiet engine E. At the turbine exit, the values varied from 0.63 to 0.58, respectively.

The range of inlet blade heights obtained for the five dry turbojet turbines was considerable, extending from 2.5 inches (6.45 cm) for the 3100° F (1978 K) turbine for engine D, to 10.0 inches (25.4 cm) for the turbine for quiet engine E, as noted in table II. Exit blade heights varied from 6.2 to 10.64 inches (15.78 to 27.01 cm) between turbines D and E, respectively. The corresponding values of blade radius ratio, shown in the table, varied from 0.61 at the inlet of the turbine for the quiet engine E, to 0.90 for the 3100° F (1978 K) turbine for engine D, and varied from 0.59 to 0.77 at the exit of these two turbines, respectively.

In general, the blade heights for the five dry turbojet turbines decreased with increasing turbine inlet temperature, caused by a corresponding decrease in compressor and turbine weight flow and a corresponding increase in turbine inlet pressure with increasing compressor pressure ratios. Inlet blade heights decreased more rapidly than exit blade heights as turbine inlet temperatures increased because of a rapid increase in the amount of cooling air bypassing the turbine inlet, and because of an increase in turbine pressure ratios, as will be shown later. The ratio of outlet-to-inlet turbine blade height for the quiet engine E was approximately 1.06, whereas the ratio was approximately 2.45 for the 3100° F (1978 K) turbine for engine D.

Axial critical velocity ratio. - The near uniformity in axial critical velocity ratio that was achieved in the design of the turbines for the three afterburning turbojet engines E, F, and G is noted in table II. The values varied from 0.25 to 0.28 at the turbine inlet, accelerating to values of 0.37 to 0.39 at the inlet to the second stage, and to values of 0.43 to 0.45 at the turbine exit (second-stage exit). These values were considered to be consistent with present design practice. The axial acceleration of the flow was close to uniform from turbine inlet to exit.

Table II also shows the near uniformity in turbine axial critical velocity ratio that was achieved between the turbines designed for the five dry turbojet engines A to E.

The values varied from 0.23 to 0.25 at the turbine inlet, from 0.36 to 0.38 at the inlet to the second stage, and from 0.50 to 0.52 at the turbine exit. The level of values entering the first and second stages matched closely with those obtained for the three afterburning turbojet turbines. However, with no afterburner to restrict the level of turbine exit critical velocity ratio to values of approximately 0.45, as was arbitrarily assumed for the afterburning turbojet turbines, the ratio was allowed to increase by an average of 0.06 to the moderately high values shown. This resulted in approximately a linear acceleration in the axial critical velocity ratio from inlet to exit of the turbines for the five dry turbojet engines.

The validity of the assumption that a higher level of turbine exit critical velocity ratio could be used for the dry turbojet engines could not be compared with experience because none existed at the higher levels of turbine inlet temperature investigated. However, it was noted that in assuming a constant level of turbine exit critical velocity ratio over the range of turbine inlet temperatures considered, pressure losses in the exhaust ducting between the turbine exit and jet nozzle would not vary appreciably because, as will be shown later, turbine exit temperatures and, therefore, exit flow velocities did not vary appreciably.

Cooling requirements. - The total cooling airflow ratio found necessary to convectively cool the blading, and to film cool the hub and tip walls of the turbines for the three afterburning turbojet engines, is shown in figure 5 for the assumed values of blade thermal cooling effectiveness Λ, and cooling air temperature reduction $\Delta T'_{HX,\,y}$ of 0.70 and 400° F (222 K), respectively. A cooling airflow ratio y' of 0.070 was required to cool the two turbines designed for noisy engines G and F, while a value of 0.064 was required to cool the turbine designed for the quiet engine E. The lower value was due primarily to the lower compressor pressure ratio of the quiet engine, and hence to lower heat-transfer coefficients, as will be shown later, and to a lower temperature of the cooling air used to cool the turbine $\left[T'_y = 655^{\circ}\text{ F (620 K) for the quiet engine compared to } 744^{\circ}\text{ F (670 K) for the two noisy engines F and G at cruise}\right]$. It may also be noted on the figure that the resulting values of the turbine cooling airflow ratio for the afterburning turbojet engines agreed closely with the value of 0.06 noted in table I and used in the reference studies (refs. 1 and 2) to size the engines and aircraft, and to determine payloads.

The total cooling airflow ratios found necessary to cool each of the turbines for the five dry turbojet engines, using the same method of cooling noted previously for the three afterburning turbojet turbines, are also shown in figure 5 for the assumed values of blade thermal cooling effectiveness Λ, and cooling air temperature reduction $\Delta T'_{HX,\,y}$, of 0.70 and 400° F (222 K), respectively. The two 2200° F (1478 K) turbines for engines A and E required approximately the same cooling airflow ratio (0.067) as the corresponding turbines for the afterburning turbojet engines E, F, and G. However,

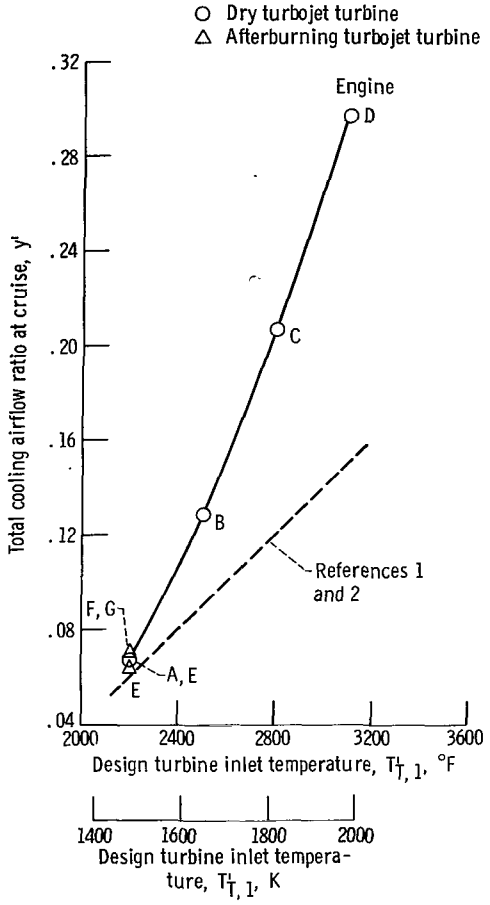

Figure 5. - Total turbine cooling airflow ratios. Pattern factor, 0.15; blade thermal cooling effectiveness, 0.70; cooling air temperature reduction across the cooling air heat exchanger, 400° F (222 K).

the turbine cooling airflow ratios required for engines B, C, and D increased nearly linearly with turbine inlet temperature to values of 0.13, 0.21, and 0.30 for the 2500°, 2800°, and 3100° F (1645, 1811, and 1978 K) turbines. It may be noted in table I and in figure 5 that the latter three cooling airflow ratios did not agree with the values of 0.09, 0.12, and 0.15 that were assumed and used in the analyses of references 1 and 2. The differences were larger at the higher turbine inlet temperatures, and cast some doubt on the weight flow of the engines used herein, and, therefore, on the size of the designs evolved for these three turbines. However, it was determined that the other aspects of the turbine designs would not be affected by this difference in size. Note, for instance, the almost negligible difference in compressor-to-turbine tip diameter ratio, turbine blade radius ratio, and total cooling airflow ratio that was obtained between the turbines designed for the two noisy afterburner turbojet engines F and G.

These latter two engines differed by approximately 25 percent in weight flow and size. Therefore, for this reason, the design details of the turbines for engines B, C, and D were determined at the values of engine weight flow obtained from references 1 and 2 in spite of the large differences in cooling airflow ratios used.

Effect of coolant assumptions. - The design characteristics of the turbines described in figures 4 and 5 and table II were evolved for the assumed values of blade thermal cooling effectiveness Λ, and cooling air temperature reduction $\Delta T'_{HX,y}$ of 0.70 and 400° F (222 K), respectively. In order to determine the effect of this assumption on turbine cooling airflow ratios as well as on the other aspects of the turbine design, a range of Λ of from 0.50 to 0.70 and $\Delta T'_{HX,y}$ of from 0° to 400° F (222 K), or in one case 600° F (333 K), was assumed for one of the afterburning and one of the dry turbojet turbines. The results are shown in figure 6.

The variation in total cooling airflow ratio with Λ and $\Delta T'_{HX,y}$ for the

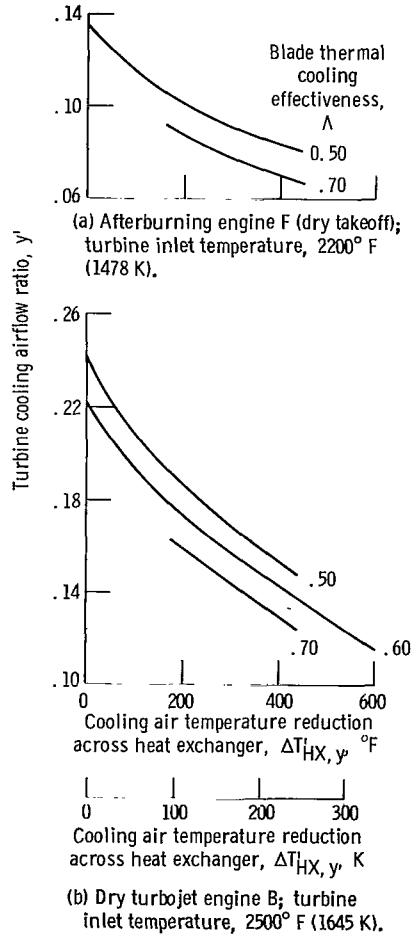

Figure 6. - Effect of blade thermal cooling effectiveness and cooling air temperature reductions on turbine cooling airflow ratio. Pattern factor, 0.15.

intermediate-size afterburning turbojet, designated engine F in table I and designed to takeoff dry, is shown in figure 6(a). Reducing Λ from 0.70 to 0.50 at a $\Delta T'_{HX,y} = 400^{\circ}$ F (222 K), increased the cooling airflow ratio from the value shown in figures 5 and 6(a) of 0.070 to 0.083, but eliminating the cooling air heat exchanger completely ($\Delta T'_{HX,y} = 0$) increased the ratio considerably to 0.135.

For the dry turbojet turbine selected, designated engine B in table I [2500° F (1645 K) turbine inlet temperature] and shown in figure 6(b), the same general trends were observed but at a higher level of cooling airflow ratio. Reducing Λ from 0.70 to 0.50 at a $\Delta T'_{HX,y} = 400^{\circ}$ F (222 K), increased the cooling airflow ratio from the value shown in figures 5 and 6(b) of 0.129, to 0.152, but eliminating the cooling air heat exchanger completely caused a further increase in the ratio to 0.241. A 600° F (333 K) increase in the temperature of the cooling air at a value of Λ of 0.60 increased the ratio from 0.115 to 0.222. A further discussion of the effects of these two variables on the cooling airflow ratio is presented in the section Cooling requirements.

Aerodynamic and Thermodynamic Characteristics

A detailed description of the aerodynamic and thermodynamic characteristics of the eight turbines, determined at the cruise condition of Mach 3 at 70 000 feet (21 350 m), is presented in figures 7 to 13 and table III, and is discussed in the following three sections on overall requirements, exit state conditions, and velocity diagram characteristics.

Overall requirements. - Plots of turbine specific work, total-pressure ratio, blade speed, and work parameter are shown plotted in figures 7 and 8 for values of $\Lambda = 0.70$ and $\Delta T'_{HX,y} = 400^{\circ}$ F (222 K). They are plotted as a function of turbine exit weight flow for the afterburning turbojet turbines in figure 7, and turbine inlet temperature for the dry turbojet turbines in figure 8. The symbols indicate the engine designation and associated level of jet noise at takeoff. Figure 7(a) shows the decrease in turbine specific work Δh_T from 142 and 141 to 115 Btu per pound (330 and 328 to 267 J/g) between the turbines for the two noisy engines F and G; and the turbine for the quiet engine E. The decrease between the latter two turbines reflects the decrease in design compressor pressure ratio from 10.0 to 8.0. The relations and assumptions used to determine Δh_T are discussed in appendix C.

Figure 7(b) shows the corresponding values of turbine equivalent specific work $(\Delta h/\theta_1)_T$. The values ranged from 28.4 Btu per pound (66.1 J/g) for the turbines for the two noisy engines F and G, to 23.1 Btu per pound (53.8 J/g) for the turbine for the quiet engine E.

The effect of turbine specific work on turbine total pressure ratio at the assumed

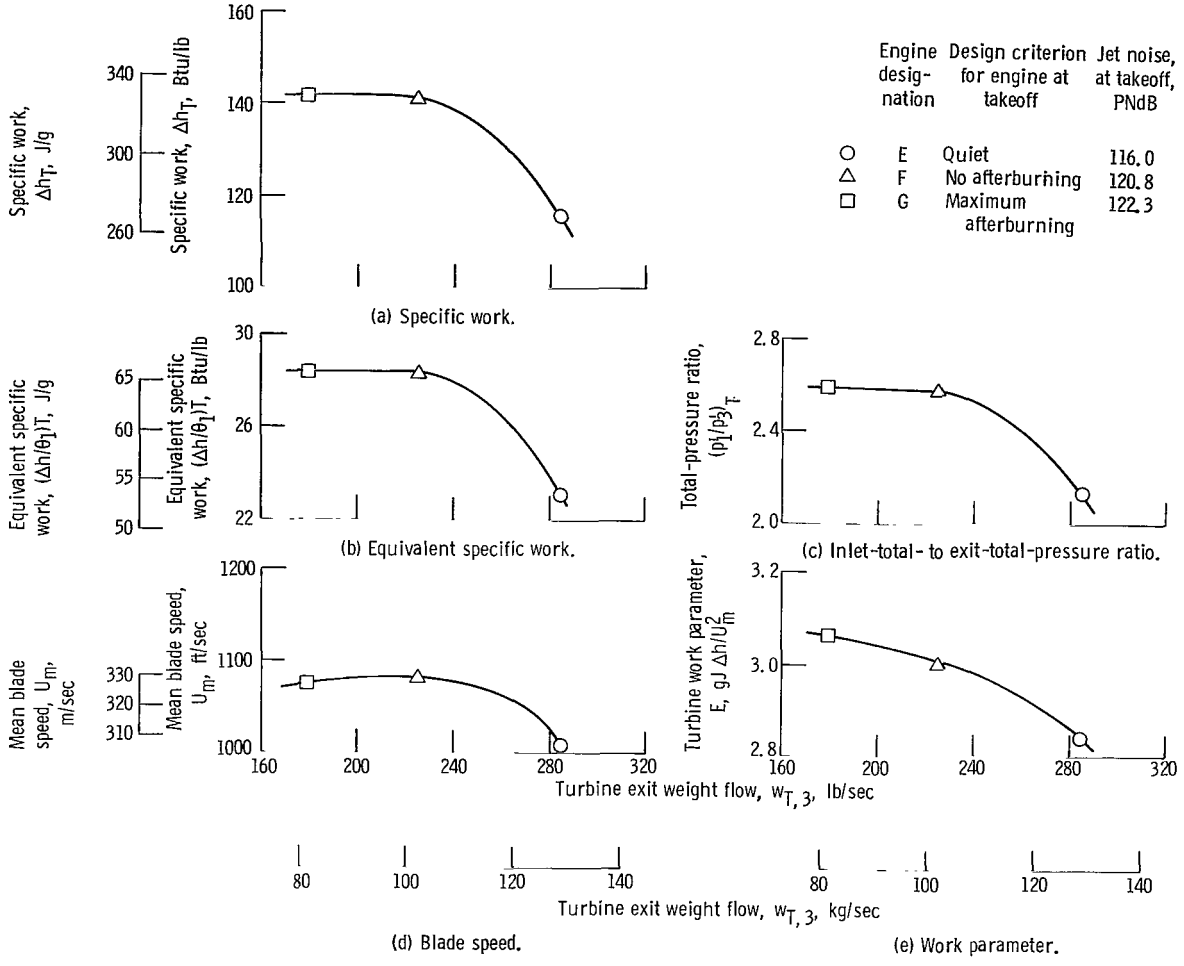

Figure 7. - Effect of engine design requirements on turbine flow, work, loading, speed, and pressure ratio for the afterburning turbojet engines at cruise. Design turbine inlet temperature, 2200° F (1478 K); pattern factor, 0.15; blade thermal cooling effectiveness, 0.70; cooling air temperature reduction across the cooling air heat exchanger, 400° F (222 K).

turbine efficiency of 0.90 is shown in figure 7(c). The ratio varied from approximately 2.6 for the two noisy turbojets F and G to 2.1 for the quiet turbojet E. This reduction in turbine total-pressure ratio was caused by the reduction in turbine specific work which was due, in turn, to the reduction in compressor pressure ratio and turbine cooling airflow ratio.

The rotor blade speeds found necessary to satisfy the specific work and rotor hub reaction requirements are shown plotted in figure 7(d). Mean blade speeds were essentially the same for the two noisy turbojet turbines at 1075 and 1080 feet per second (328 and 329 m/sec), but decreased to 1010 feet per second (308 m/sec) for the quiet turbojet because of the reduction in turbine specific work. Corresponding values of

equivalent mean blade speed $(U_m/\sqrt{\theta_1})_T$ were 481, 484, and 451 feet per second (147, 148, and 138 m/sec).

Finally, the combined effect of turbine specific work and mean blade speed on the turbine work parameter E is shown in figure 7(e) for the three turbines. The turbine work parameter decreased slightly from 3.07 to 3.01 in going from the smaller to larger noisy engines because of the slight increase in turbine mean blade speed. However, the turbine work parameter for the quiet turbojet turbine decreased to 2.84, reflecting a larger decrease in specific work compared to the decrease in mean blade speed. These values of E were generally higher than the corresponding values obtained in appendix B, wherein a simplified method was used to determine E and the number of stages required for the turbines. The values of E were higher primarily because of the higher value of equivalent mean blade speed arbitrarily assumed in the appendix of 500 feet per second (152 m/sec), compared to the values obtained for the three turbines, as noted in the discussion of figure 7(d). However, the increase in E was not sufficient to alter the conclusion noted in the appendix that two-stage turbines best met the requirements for these three engines.

Figure 8(a) shows the marked increase in turbine cruise specific work with increasing turbine inlet temperature for the dry turbojet engines A to D. The values increased from 121 to 285 Btu per pound (281 to 662 J/g) over the range of turbine inlet temperatures investigated for the noisy engines, and was approximately the same as noted before in figure 7(a) for the quiet turbojet turbine E of 116 Btu per pound (270 J/g). The increase in specific work with temperature reflects not only the increase in design compressor pressure ratio from 8.35 to 19.0, but a decrease in the turbine-to-compressor weight flow ratio available for doing work. The latter effect was caused by the increase in the turbine cooling airflow ratio from 0.067 to 0.30.

Figure 8(b) shows the corresponding values of turbine equivalent specific work. The values ranged from 23 Btu per pound (53.4 J/g) for the quiet turbojet turbine E, to 24 Btu per pound (55.8 J/g) for the low-temperature noisy turbojet A, to 29, 35, and 43 Btu per pound (67, 81, and 100 J/g) for the 2500°, 2800°, and 3100° F (1645, 1811, and 1978 K) turbines of engines B, C, and D, respectively.

The combined effect that the variation in turbine specific work, turbine inlet temperature, and the assumed turbine efficiency has on turbine total-pressure ratio is shown in figure 8(c). The ratios varied from 2.1 to 2.2 for the two lower-temperature turbines A and E, which were close to the ratio required for the quiet afterburning turbojet E, to ratios of 2.7, 3.4, and 4.6 for the three higher-temperature turbines B, C, and D. The total-pressure ratio for the last turbine, 4.6 for a turbine inlet temperature of 3100° F (1978 K), might be considered too high for a two-stage turbine. However, as will be shown later, the blade turning angles, blade leaving velocities, and wall flare angles obtained for this turbine were reasonable.

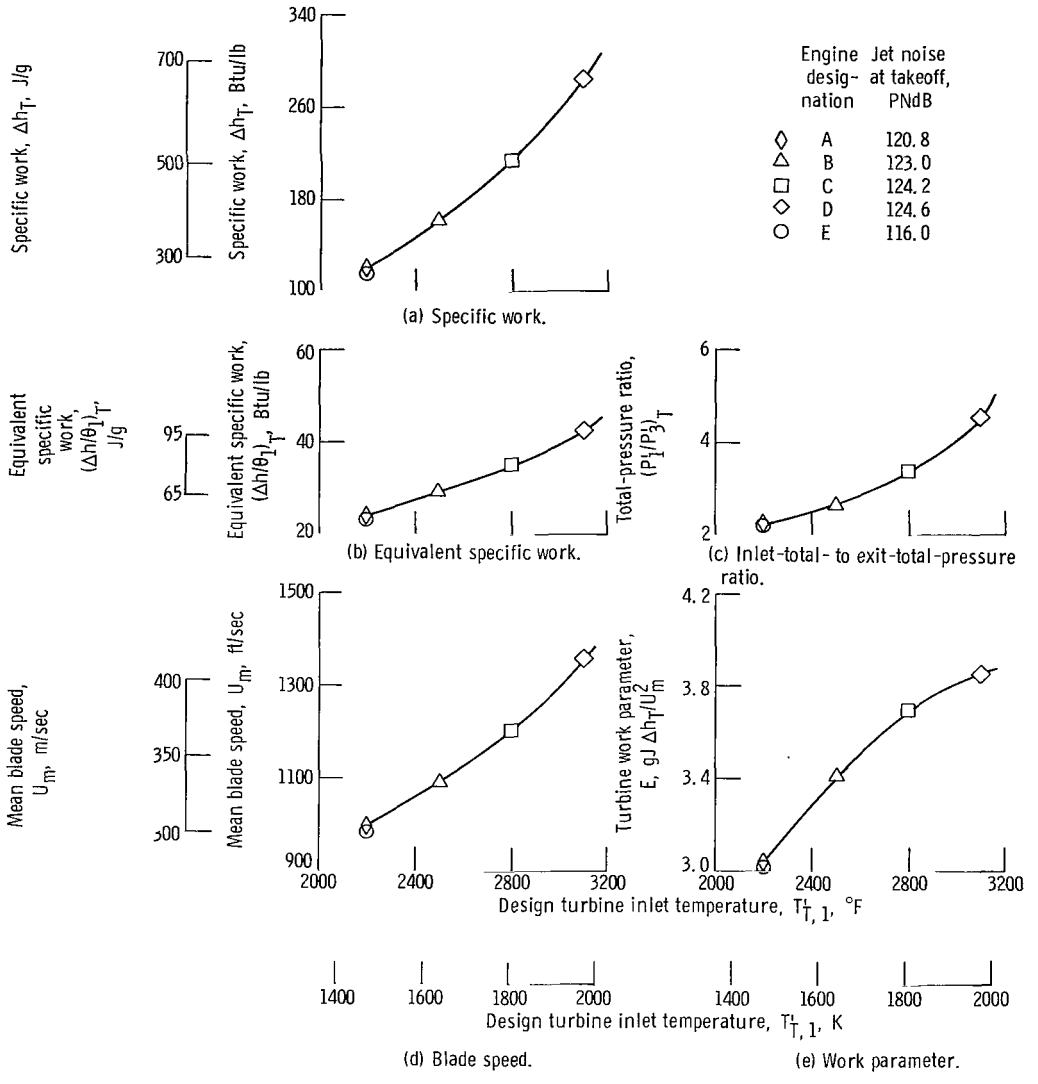

Figure 8. - Effect of engine design requirements on turbine flow, work, loading, speed, and pressure ratio for the dry turbojet engines at cruise. Pattern factor, 0.15; blade thermal cooling effectiveness, 0.70; cooling air temperature reduction across the cooling air heat exchanger, 400° F (222 K).

The rotor blade speeds found necessary to satisfy the specific work and rotor hub reaction requirements are shown in figure 8(d) for the five dry turbojet turbines. Mean blade speeds varied upward from the relatively low values of 980 and 1000 feet per second (299 and 304 m/sec) for the quiet and noisy 2200° F (1478 K) turbojets A and E, to values of 1090, 1200, and 1360 feet per second (332, 366, and 415 m/sec) for the 2500°, 2800°, and 3100° F (1645, 1811, and 1978 K) noisy turbojets B, C, and D. Corresponding values of equivalent mean blade speed $\left(U_m/\sqrt{\theta_1}\right)_T$ were 438, 446, 463, 487, and 526 feet per second (134, 136, 141, 149, and 160 m/sec). Because of the fixed com-

pressor tip speed of 1300 feet per second (396 m/sec) assumed in the analysis, the high level of turbine blade speed required for the higher-temperature turbines resulted in turbine tip diameters that exceeded the tip diameter of their respective compressors, as was noted in figure 4. Also noted in figure 8(d) is the slightly lower blade speed that was required for the quiet turbojet turbine E, compared to the corresponding afterburning turbojet turbine E.

Finally, the combined effect of turbine specific work and mean blade speed on the turbine work parameter E is shown in figure 8(e) for the five dry turbojet turbines. The values of E of 3.01 obtained for the quiet turbojet turbine was larger than the value of 2.84 obtained for the corresponding afterburner turbojet turbine because of the reduction in blade speed. The value increased slightly for the low-temperature noisy engine A to 3.04, and then increased rapidly to values of 3.41, 3.69, and 3.85 for the 2500°, 2800°, and 3100° F (1645, 1811, and 1978 K) turbines for engines B, C, and D.

As in the case of the three afterburning turbojet turbines noted in figure 7(e), these values of E were generally higher than the corresponding values obtained in appendix B, and were used therein to determine the number of turbine stages for each turbine. However, the maximum value of E of 3.85 required for the turbine of engine D was within the capability of the two-stage turbine noted in reference 4, and therefore did not alter the conclusion noted in the appendix that two-stage turbines could best meet the requirements for the five dry turbojet turbines.

Figure 9 shows the effect that varying Λ and $\Delta T'_{HX,\,y}$ had on the total-pressure ratio required for the two turbines of engines B and F noted previously in figure 6. The effect of these two variables on pressure ratio for the 2200° F (1478 K) afterburning turbojet turbine F was not as large as might be expected, varying from 2.58 to 2.73 over the range of variables noted in figure 9(a). The effect was due to the variation in cooling airflow ratio (shown in fig. 6(a)), which doubled from 0.070 to 0.135 over the range of Λ and $\Delta T'_{HX,\,y}$ considered. However, the amount of work recovered from the cooling air increased as $\Delta T'_{HX,\,y}$ decreased because of the assumption made in appendix C that the equivalent specific work of the cooling air equaled one-half the equivalent specific work of the main gas stream. Therefore, as the temperature of the cooling air increased with decreasing values of $\Delta T'_{HX,\,y}$, the specific work output of the cooling air increased.

The effect of varying Λ and $\Delta T'_{HX,\,y}$ on the pressure ratio of the 2500° F (1645 K) dry turbojet turbine B is shown in figure 9(b). The effect is much larger than for turbine F because, as shown in figure 6(b), the cooling airflow ratio was nearly double. The pressure ratios varied from 2.67 to 3.05 over the range of variables noted in figure 9(b). The effect of varying just Λ on turbine pressure ratio reflected the effect of varying the ratio of gas-to-cooling airflow available for doing work across the turbine. An increase in Λ caused approximately twice the decrease in turbine pressure ratio for engine B as for engine F.

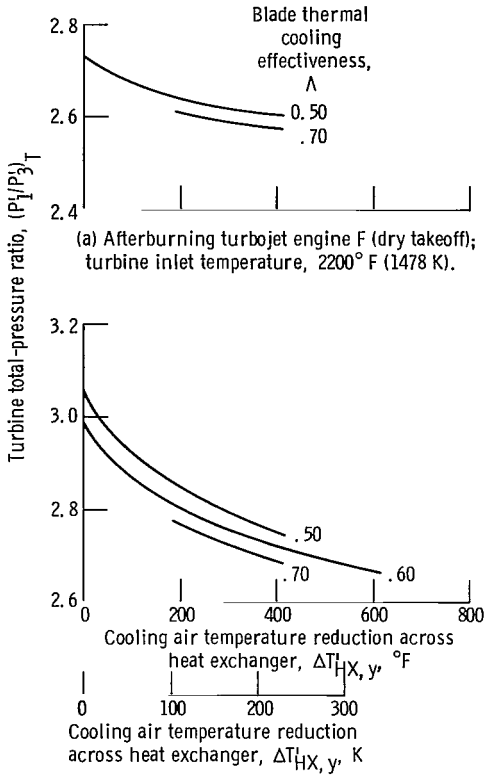

(a) Afterburning turbojet engine F (dry takeoff); turbine inlet temperature, 2200° F (1478 K).

(b) Dry turbojet engine B; turbine inlet temperature, 2500° F (1645 K).

Figure 9. - Effect of blade thermal cooling effectiveness and cooling air temperature reduction on turbine pressure ratio at cruise. Pattern factor, 0.15.

Exit state conditions. - The variation in turbine exit total pressure and temperature is shown plotted in figures 10(a) and (b) as a function of turbine exit weight flow for both types of engines investigated. The values presented are at Mach 3 cruise at 70 000 feet (21 350 m), as noted previously, and are applicable only to the level of compressor pressure ratios and cooling airflow ratios considered in the analysis. The symbols and line quality identify the type of engine and inlet temperature of the turbines. Also shown on the figures for comparison are the corresponding values of exit total pressure and temperature obtained from the analysis of references 1 and 2.

It may be seen in figure 10(a) that there was essentially no variation in exit total pressure between the five 2200° F (1478 K) turbines, even though the design compressor pressure ratio varied from 10.0 for the two noisy afterburning turbojets F and G, to 8.0 for the two quiet turbojets E, to 8.35 for the noisy dry turbojet A. Exit total pressures did vary, however, at the elevated turbine inlet temperatures investigated, reaching a peak of 28.8 psia (19.9 N/cm^2) at a temperature of 2800° F (1811 K) for engine C, and then decreasing to 27.3 psia (18.8 N/cm^2) at 3100° F (1978 K) for engine D. This

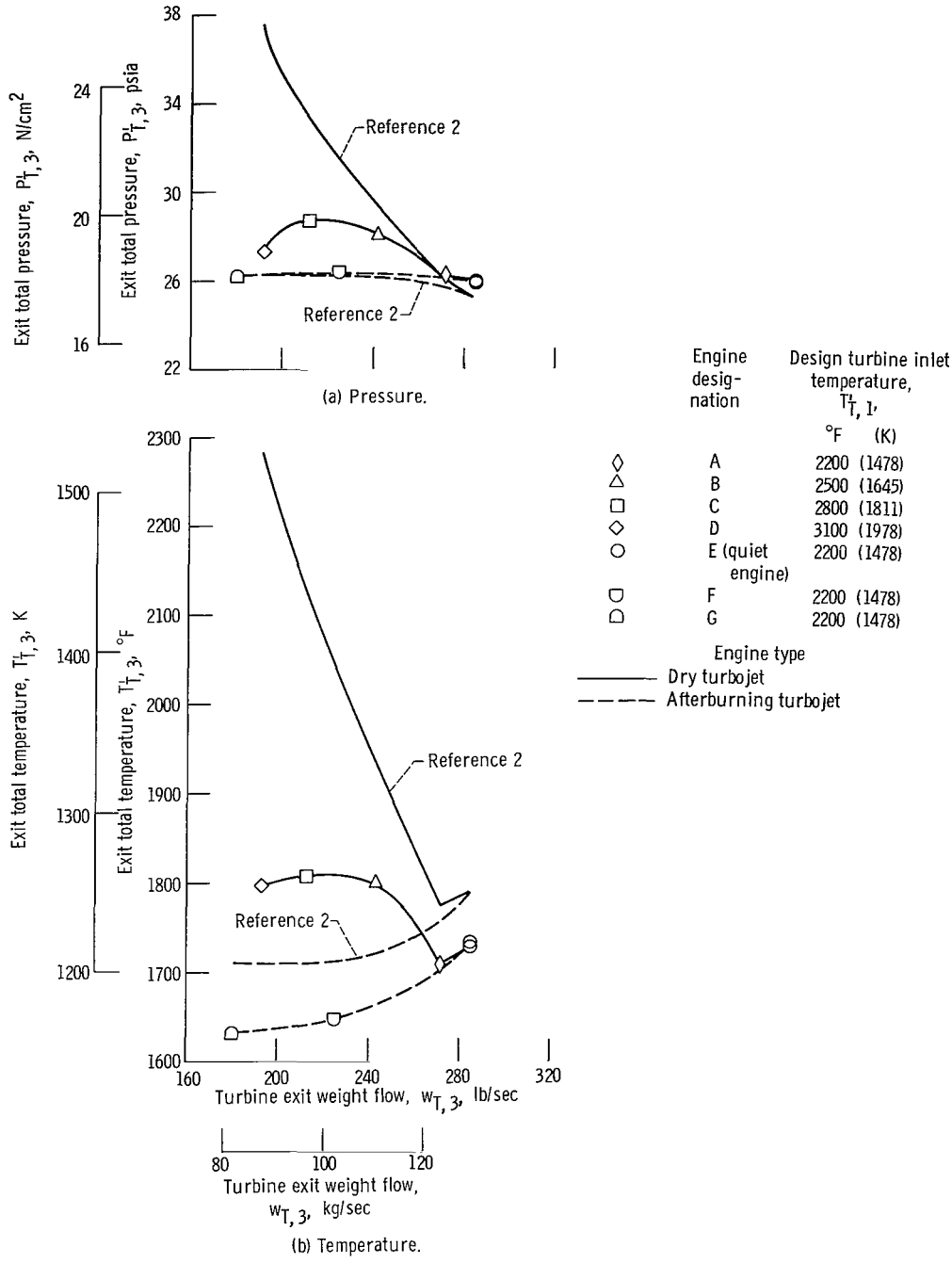

Figure 10. - Effect of engine design requirements on turbine exit flow conditions at cruise. Pattern factor, 0.15; blade thermal cooling effectiveness, 0.70; cooling air temperature reduction across the cooling air heat exchanger, 400° F (222 K).

occurred even though compressor pressure ratio continued to increase from 14.75 to 19.00 between engines C and D, respectively.

Figure 10(b) shows the corresponding values of turbine exit temperature $T'_{T,3}$. Exit temperatures increased with increasing turbine exit weight flow for the five 2200° F (1478 K) turbines because of the corresponding decrease in compressor pressure ratio, and, therefore, the decrease in turbine specific work. Over the range of turbine exit weight flows covered at cruise from 180 to 285 pounds per second (82 to 129 kg/sec) for these five turbines, turbine exit temperature increased from 1630° to 1730° (1161 to 1218 K), while compressor pressure ratio decreased from 10.0 to 8.0. The 15° F (8.3 K) difference in turbine exit temperature between the two noisy turbojets F and G was due primarily to the slight difference in cooling airflow ratio.

Figure 10(b) also shows that there was essentially no variation in turbine exit temperature for the three higher temperature turbines for engines B, C, and D. Temperatures averaged 100° F (55.6 K) higher than for the 2200° F (1478 K) dry turbojet turbine A. Above a turbine inlet temperature of approximately 2700° F (1757 K), no further increase in turbine exit temperature was possible because of the increase in turbine specific work caused by the increase in compressor pressure ratio and turbine cooling airflow ratio, and because of the quenching effect of the cooling air.

The level of total pressure and temperature leaving the turbine and entering the afterburner or jet nozzle is of prime importance in determining the specific thrust and specific fuel consumption for the engines. The higher the pressure and temperature, the higher the nozzle exit velocity and specific gross thrust. However, when the effect of propulsion efficiency is considered, a limiting value of turbine exit pressure and temperature can be determined which will maximize the specific net thrust or minimize the specific fuel consumption. The turbine designs developed in this report were for engines which were sized to values of compressor weight flow and pressure ratio which either maximized payload, met certain noise constraints at takeoff, or met thrust requirements at transonic acceleration. However, because of the difference between the values of cooling airflow ratio and specific work used in the analyses of references 1 and 2, and those obtained herein for the three high-temperature turbines B, C, and D, a reduction in turbine exit total pressure and temperature from the values obtained in references 1 and 2 resulted. The magnitude of this reduction in pressure and temperature was noted in figures 10(a) and (b). Results of the present analysis indicate that, if convection cooling is used for the turbine blades and vanes, no further increase in engine specific thrust or payload would be likely beyond a turbine inlet temperature of 2700° to 2800° F (1757 to 1811 K). And, in fact, there may be little advantage in going beyond a turbine inlet temperature of 2500° F (1645 K). However, because this conclusion applies to only the particular engine types, compressor pressure ratios, metal temperatures, methods of cooling (convection cooling of the turbine blades and film

cooling of the hub and tip walls), and other assumptions used in this analysis, it did not detract from the implied objective of the analysis of determining the design characteristics of the turbines over a range of turbine inlet temperatures.

An additional factor may also be noted in figure 10(b): The deficit in turbine exit temperature between the values used in the analyses of references 1 and 2 and those obtained for the five 2200° F (1478 K) turbines A, E, F, and G. The deficit was due in part to the small increase in cooling airflow ratio required for the five turbines (0.064 to 0.070, compared to 0.60 used in refs. 1 and 2), and in part to the quenching effect of the 400° F (222 K) reduction in cooling air temperature used herein but not considered in references 1 and 2. The effect of this reduction in cooling air temperature was also a factor in the deficit in turbine exit temperature for the higher temperature turbines of engines B, C, and D shown in figure 10(b) and those used in reference 2. However, as noted previously, the deficit was aggravated for the higher-temperature turbines by the large increase in cooling airflow ratios compared to the values used in references 1 and 2.

In the case of the three afterburning turbojet engines E, F, and G, the reduced level of turbine exit temperature could have been compensated for by an increase in the temperature rise across the afterburner. Thus, engine specific thrust could have been restored. In the case of the five dry turbojet engines, the effect of the reduced level of turbine exit temperature on reducing engine specific thrust could only have been compensated for by increasing engine weight flow. This would have increased both engine weight and engine drag. Either an increase in the afterburner temperature or engine weight and drag would have a tendency to reduce the aircraft payload, as indicated in references 1 and 2.

References 1 and 2 did not account for the effects that reducing the temperature of the cooling air had on the turbine exit conditions. However, references 1 and 2 also did not account for a decrease in the engine specific fuel consumption that would occur from increasing the temperature of the gaseous fuel entering the burner, which increases the sensible heat and thus the heating value of the fuel. The balancing effects were considered beyond the scope of references 1 and 2. Reference 3 did consider the effect of sensible heat increases which resulted in a decrease in specific fuel consumption. Therefore, it should be noted that although a deficit in turbine exit temperature (or reduction in engine specific thrust) exists in this report, this deficit may be offset by a decrease in the fuel required to fly the mission because of an inherent decrease in engine specific fuel consumption. The exact effect that this combination of effects would have on payload, which is a direct function of the amount of fuel used for the mission, was considered beyond the scope of this report.

Finally, the effect of varying Λ and $\Delta T'_{HX,y}$ on turbine exit temperature is shown in figure 11 for the 2500° F (1645 K) turbine of engine B. The figure indicates that tur-

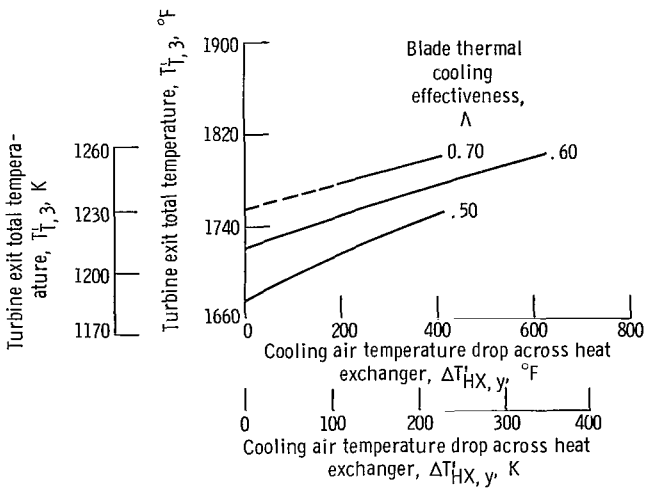

Figure 11. - Effect of blade thermal cooling effectiveness and cooling air temperature reductions on turbine exit total temperature for the 2500° F (1645 K) dry turbojet engine B. Pattern factor, 0.15.

bine exit temperature increased as the temperature (and hence the amount) of the cooling air was reduced. At a value of Λ of 0.60, turbine exit temperatures increased 80° F (44.5 K) when the cooling air temperature drop across the heat exchanger was increased from 0° to 600° F (333 K). The rate at which the turbine exit temperature varied with $\Delta T'_{HX,y}$ increased as Λ decreased. A cooling air temperature reduction of 400° F (222 K) caused the turbine exit temperatures to increase by 46°, 56°, and 70° F (25.5, 31.1, and 38.9 K) as values of Λ decreased from 0.70 to 0.60 and to 0.50, respectively. The increase in the rate of change of turbine exit temperature with $\Delta T'_{HX,y}$ as Λ decreased reflected the increase in the amount of cooling air required.

Velocity diagram characteristics. - The free-stream critical velocity ratios and flow angles into and out of each turbine blade row are tabulated in table III for all eight turbines. Accurate knowledge of these quantities was required to compute blade surface areas and cooling airflow requirements for the blading. Also, as noted in the INTRODUCTION, the information will be useful in support of future research efforts investigating both the heat-transfer characteristics of turbines and the heat-sink capability of methane fuel for turbine cooling. All information noted in this section was derived for values of $\Lambda = 0.70$, PF = 0.15, and $\Delta T'_{HX,y} = 400^{\circ}$ F (222 K).

A level of critical velocity ratio of approximately 0.25 and 0.40 was obtained at the inlet of all first and second-stage stators, respectively. The values at the inlet to the first stage were axial and, therefore, equal to the values indicated in table II. Values at the stator exit of both stages varied considerably from an average of 0.77 for the two 2200° F (1478 K) high-specific-work turbines for the noisy afterburning turbojets F and G, to approximately 0.67 for the two quiet turbojets E, to approximately 0.70 for

TABLE III. - TURBINE VELOCITY DIAGRAM AND BLADE LOADING CHARACTERISTICS

Characteristic	Engine designation[a]															
	A		B		C		D		E		E		F		G	
	Stage number															
	1	2	1	2	1	2	1	2	1	2	1	2	1	2	1	2
	Engine type															
	Dry turbojet										Afterburning turbojet					
Design turbine inlet temperature, $T'_{T,1}$, ^{o}F (K)	2200 (1478)		2500 (1645)		2800 (1811)		3100 (1978)		2200 (1478)							
Mean absolute velocity ratio, $(V/V_{cr})_m$:																
Inlet	0.24	0.38	0.25	0.41	0.23	0.40	0.23	0.41	0.24	0.39	0.28	0.40	0.25	0.38	0.26	0.39
Outlet	.69	.71	.81	.82	.93	.93	1.06	1.05	.66	.70	.70	.69	.79	.74	.79	.76
Mean relative velocity ratio, $(W/W_{cr})_m$:																
Inlet	0.36	0.43	0.45	0.51	0.52	0.56	0.62	0.62	0.34	0.45	0.39	0.44	0.42	0.43	0.43	0.45
Outlet	.68	.71	.71	.75	.75	.79	.81	.84	.68	.71	.67	.68	.69	.69	.69	.71
Angle of absolute velocity from axial direction for stator, $\alpha_{s,m}$:																
Inlet	0	-20.3	0	-19.2	0	-21.5	0	-23.1	0	-21.3	0	-15.2	0	-14.7	0	-15.8
Outlet	64.2	53.2	66.9	56.4	68.8	60.0	69.1	63.5	63.8	52.1	60.8	51.3	65.1	57.9	64.7	57.1
Angle of relative velocity from axial direction for rotor, $\alpha_{r,m}$:																
Inlet	31.0	14.3	42.3	23.4	48.6	31.2	50.6	37.1	28.9	13.0	26.6	9.1	35.4	17.6	35.6	18.5
Outlet	-58.7	-46.7	-58.3	-47.5	-60.8	-49.3	-62.8	-53.0	-58.8	-45.5	-55.5	-49.3	-58.7	-53.2	-58.6	-51.2
Aerodynamic (tangential) stator blade loading coefficient, [b] ψ_s	0.73	1.06	0.65	0.96	0.59	0.85	0.58	0.75	0.74	1.09	0.83	1.11	0.70	0.92	0.72	0.94

[a] See table I for details.

[b] $\psi_r = 1.0$.

the 2200° F (1478 K) noisy dry turbojet A. From there, the exit free-stream critical velocity ratios increased rapidly with increasing turbine inlet temperature (and specific work) to values of 0.82, 0.93, and 1.05 for turbine inlet temperatures of 2500°, 2800°, and 3100° F (1645, 1811, and 1978 K), respectively. (The value of 1.05 exceeded by a small amount the arbitrary limit of 1.00 set in appendix D.) All values were essentially independent of stage number with the exception of the stator exit values for the 2200° F (1478 K) turbines which all had slightly higher first-stage values than second stage.

Rotor inlet and exit relative free-stream critical velocity ratios for the three afterburning turbojet turbines E, F, and G were approximately 0.43 and 0.70, respectively, for both stages, with some divergence between the first- and second-stage inlet values for the quiet engine E. Rotor inlet values for the dry turbojet turbines were more dependent on stage number, varying from 0.35 for the two 2200° F (1478 K) turbines A and E to 0.62 for the 3100° F (1978 K) turbine D, and from 0.44 to the same value of 0.62, respectively, for the second stage. Corresponding exit values varied from approximately 0.70 to 0.82, with the second-stage values only slightly above the first-stage. In all cases, the difference between rotor mean-radius inlet and exit critical velocity ratio was indicative of the constant values of rotor hub reaction $\mathscr{R}_h$, assumed for each rotor of the eight turbines, as discussed in appendix D.

The deviation of stator inlet free-stream angle from axial for the first stage was 0° (for axial entry), and approximately 15° and 20° for the second stage of the afterburning and dry turbojet turbines, respectively. First-stage stator exit angles varied from 61° to 65° from axial for the five 2200° F (1478 K) turbines, and from 66° to 69° from axial for the 2500° to 3100° F (1645 to 1978 K) turbines B, C, and D. The total variation in exit flow angle from the tangential direction was, therefore, from 21° to 29°. Second-stage stator exit free-stream angles averaged approximately 8° less than the first stage for the two noisy afterburning turbojet turbines F and G and the two high-temperature dry turbojets C and D, and approximately 10° less for the remaining turbines.

The deviation of the rotor relative inlet free-stream angle from axial varied widely from 10° to 50° from axial, with the variation for both stages being roughly similar to the variation in specific work between the turbines. First-stage rotor inlet angles averaged approximately 15° greater than second-stage angles. Rotor exit blade angles were more uniform between the eight turbines, averaging approximately 60° and 50° from axial for the first and second stages, respectively.

The resulting aerodynamic loading coefficients for the stator blading are also shown in table III. The coefficients, which were assumed to be linear function of stator exit angle, as noted in appendix E, were used therein to determine blade solidities and a correction factor for blade camber angle. As may be noted in table III, the coefficients varied with stator exit angle from a value of 0.58 for the first-stage stator of the highest specific work turbine D, to 1.11 for the second-stage of the lowest specific work

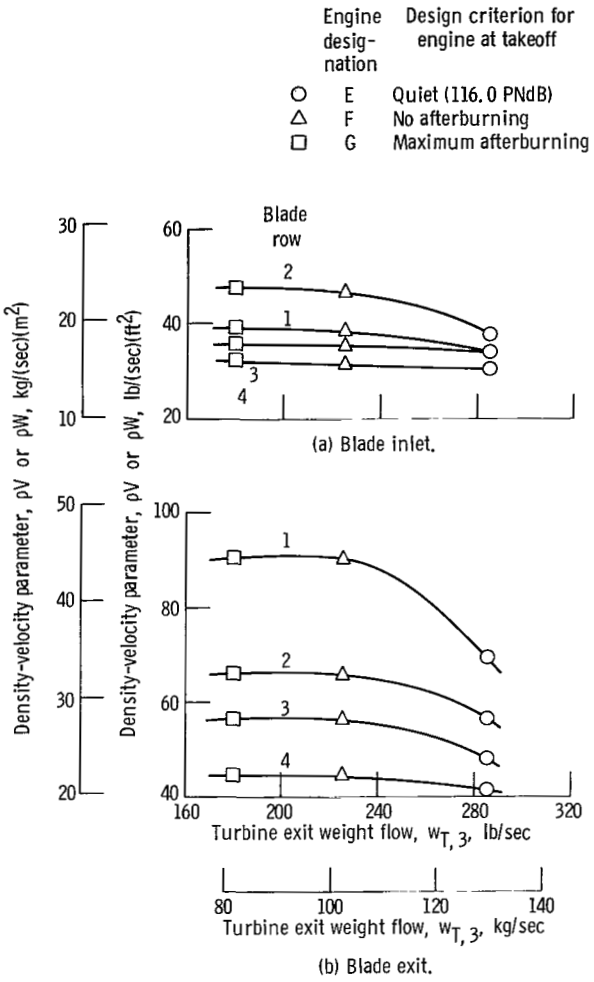

Figure 12. - Effect of engine design requirements on the blade velocity-density parameter for the afterburning turbojet turbines.

turbine E. A value of 1.0 was used for all rotor blading, as noted in table III and appendix E.

Values of the product ρV for each stator blade row and ρW for each rotor blade row are shown in figures 12 and 13 as a function of turbine exit weight flow or turbine inlet temperature for the three afterburning and five dry turbojet turbines, respectively. The product was used in the determination of blade heat-transfer coefficients and blade cooling airflow requirements, as discussed in appendix F, and was obtained from the critical velocity ratios and computed variation in total pressure and temperature across the turbines. The general level of ρV or ρW, and hence heat-transfer coefficient, shown in figure 12 for the two noisy engines F and G was higher than for the quiet engine E because of the higher compressor pressure ratio and hence turbine pressures.

Also, values increased rapidly with increasing turbine inlet temperature as shown in figure 13 for the dry turbojet turbines because of the combined effect of increasing turbine pressures and flow velocities. It may be noted in both figures that, in general, first-stage values exceeded second-stage values because of the higher level of pressure and velocity, and also that blade exit values exceeded blade inlet values because of the higher level of velocity.

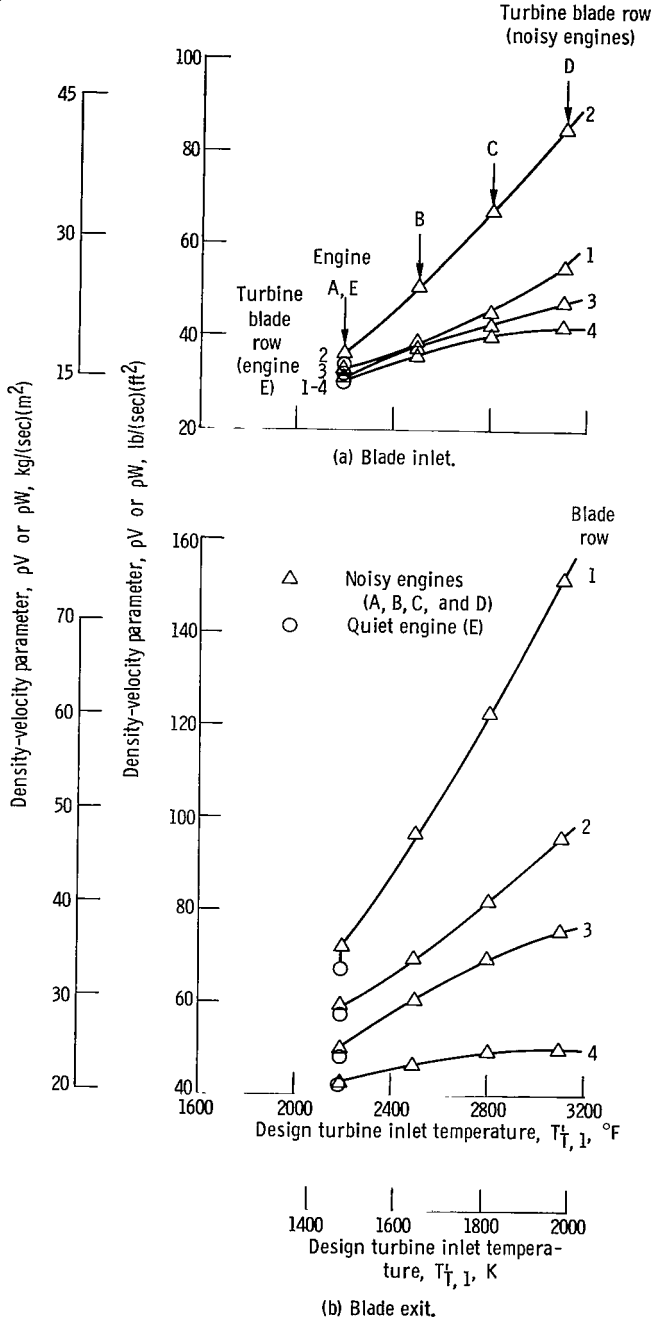

Figure 13. - Effect of engine design requirements on the blade velocity-density parameter for the dry turbojet turbines.

TABLE IV. - DIMENSIONAL

Characteristic	Engine A		Engine B		Engine C		Engine D	
	Stage 1	Stage 2	Stage 1	Stage 2	Stage 1	Stage 2	Stage 1	Stage 2
	Dry turbojet							
Turbine inlet temperature, $T'_{T,1}$, °F (K)	2200 (1478)		2500 (1645)		2800 (1811)		3100 (1978)	
Jet noise at takeoff, PNdB	120.8		123.0		124.2		124.6	
Number of blades, n:								
Stator	30	47	48	69	76	101	115	131
Rotor	50	80	88	125	129	180	171	208
Blade height at mid-chord, BH, in. (cm):								
Stator	9.02 (22.90)	9.82 (24.94)	6.04 (15.35)	7.10 (18.04)	3.99 (10.14)	5.52 (14.02)	2.54 (6.45)	4.60 (11.69)
Rotor	9.44 (23.98)	10.12 (25.72)	6.42 (16.31)	7.81 (19.84)	4.56 (11.61)	6.34 (16.10)	3.28 (8.33)	5.74 (14.59)
Axial chord, $C_{x,m}$, in. (cm):								
Stator	4.67 (11.86)	3.23 (8.20)	3.12 (7.92)	2.29 (5.82)	2.11 (5.36)	1.73 (4.40)	1.50 (3.81)	1.50 (3.81)
Rotor	3.15 (8.00)	1.99 (7.60)	2.13 (5.41)	1.49 (3.79)	1.51 (3.84)	1.17 (2.97)	1.17 (2.97)	1.10 (2.80)
Actual chord, C_m, in. (cm):								
Stator	6.18 (15.70)	3.77 (9.58)	3.96 (10.06)	2.70 (6.86)	2.60 (6.60)	2.03 (5.16)	1.84 (4.67)	1.78 (4.52)
Rotor	3.63 (9.22)	2.15 (5.46)	2.33 (5.92)	1.57 (3.99)	1.65 (4.19)	1.22 (3.10)	1.30 (3.30)	1.15 (2.92)
Blade mean camber length at mean radius, $C_{L,m}$, in. (cm):								
Stator	7.05 (17.91)	4.17 (10.60)	4.56 (11.59)	3.00 (7.62)	3.02 (7.67)	2.30 (5.84)	2.13 (5.41)	2.06 (5.24)
Rotor	4.19 (10.65)	2.33 (5.92)	2.77 (7.04)	1.74 (4.42)	2.04 (5.18)	1.38 (3.51)	1.63 (4.14)	1.34 (3.40)
Blade mean camber angle, φ_m, deg:								
Stator	40.9	31.0	38.0	32.0	35.8	31.7	35.5	32.6
Rotor	29.8	22.2	23.7	18.7	23.4	17.0	25.5	17.4
Pitch, s_m, in. (cm):								
Stator	4.29 (10.90)	2.75 (6.98)	2.78 (7.06)	1.91 (4.85)	1.83 (4.65)	1.37 (3.48)	1.31 (3.33)	1.14 (2.90)
Rotor	2.59 (6.58)	1.60 (4.07)	1.52 (3.86)	1.07 (2.72)	1.08 (2.74)	.78 (1.98)	.88 (2.24)	.72 (1.83)
Radius, ratio at mid-chord, r_h/r_t:								
Stator	0.639	0.613	0.750	0.712	0.834	0.778	0.899	0.824
Rotor	.625	.603	.736	.688	.813	.749	.871	.785
Axial aspect ratio at mid-chord, AR_x:								
Stator	1.93	3.04	1.94	3.10	1.89	3.19	1.69	3.07
Rotor	3.00	5.09	3.01	5.24	3.03	5.42	2.80	5.22
Axial solidity, $\sigma_{x,m}$:								
Stator	1.10	1.17	1.12	1.20	1.15	1.26	1.15	1.32
Rotor	1.22	1.24	1.40	1.39	1.40	1.50	1.33	1.53

[a]See table I for details.

CHARACTERISTICS OF BLADING

designation[a]							
E		E		F		G	
number							
1	2	1	2	1	2	1	2
type							
Afterburning turbojet							
2200 (1478)							
116.0				120.8		122.3	
27 45	44 77	31 55	44 77	44 72	58 87	44 73	59 94
10.03 (25.49) 10.24 (26.00)	10.45 (26.55) 10.61 (26.97)	8.63 (21.91) 9.07 (23.03)	9.74 (24.74) 10.64 (27.01)	6.27 (15.93) 6.80 (17.27)	7.84 (19.91) 8.99 (22.83)	5.49 (13.95) 6.01 (15.26)	6.86 (17.42) 7.69 (19.54)
5.13 (13.03) 3.43 (8.71)	3.45 (8.76) 2.08 (5.28)	4.40 (11.91) 3.03 (7.70)	3.22 (8.18) 2.04 (5.18)	3.20 (8.13) 2.26 (5.74)	2.57 (6.53) 1.75 (4.45)	2.80 (7.12) 1.99 (5.06)	2.25 (5.72) 1.50 (3.81)
6.84 (17.38) 3.99 (10.14)	4.00 (10.16) 2.24 (5.69)	6.19 (15.73) 3.45 (8.76)	3.79 (9.62) 2.34 (5.94)	4.18 (10.61) 2.55 (6.48)	3.10 (7.88) 1.96 (4.98)	3.68 (9.34) 2.24 (5.69)	2.70 (6.86) 1.65 (4.19)
7.80 (19.81) 4.60 (11.69)	4.42 (11.23) 2.41 (6.12)	7.08 (17.99) 3.91 (9.93)	4.11 (10.44) 2.51 (6.38)	4.74 (12.04) 2.98 (7.57)	3.44 (8.74) 2.17 (5.51)	4.17 (10.60) 2.63 (6.68)	2.99 (7.59) 1.82 (4.62)
41.4 30.8	30.4 21.6	44.7 28.5	32.9 23.4	40.0 27.6	34.0 26.7	40.4 27.3	33.5 24.4
4.75 (12.07) 2.88 (7.32)	2.93 (7.44) 1.69 (4.29)	4.24 (10.77) 2.40 (6.10)	2.97 (7.54) 1.71 (4.34)	2.91 (7.40) 1.77 (4.50)	2.21 (5.61) 1.47 (3.73)	2.56 (6.50) 1.55 (3.94)	1.93 (4.90) 1.21 (3.07)
0.608 .602	0.595 .590	0.659 .645	0.626 .601	0.733 .714	0.677 .638	0.736 .714	0.681 .649
1.96 2.98	3.03 5.10	1.97 2.99	3.03 5.21	1.96 3.01	3.05 5.14	1.96 3.02	3.05 5.13
1.08 1.19	1.18 1.23	1.04 1.26	1.08 1.19	1.10 1.28	1.16 1.19	1.09 1.28	1.17 1.24

Blade Physical Requirements

The dimensions and other physical characteristics of the turbines and blading derived for values of $\Lambda = 0.70$, PF = 0.15, and $\Delta T'_{HX, y} = 400^{\circ}$ F (222 K) are given in this section. In table IV, the following information is tabulated for the four rows of blading of all eight turbines; number of blades, blade height at mid-chord, axial and actual chord length, camber length and angle, blade pitch, mid-chord radius ratio, axial aspect ratio, and axial solidity. It was noted that as turbine inlet temperature increased, the number of blades per row increased, exceeding 100 in the fourth blade row of the 2500° F (1645 K) turbine B, and 200 in the fourth row of the 3100° F (1978 K) turbine D, where the axial chord length approached the minimum allowable value of 1 inch (2.54 cm) assumed in appendix E. Corresponding values of blade axial solidity $\sigma_{x, m}$ were 1.39 and 1.53 (the maximum value obtained for any blade row). There was essentially no difference in blade radius ratios, axial aspect ratios, or solidities between the two turbines for the noisy afterburning turbojet engines F and G. A maximum value of axial blade chord of 5.13 inches (13.03 cm) occurred in the first row of the turbine for the quiet dry turbojet E.

Axial aspect ratios fell close to the initially assumed values of 2, 3, 3, and 5 for the four blade rows for all but the highest-temperature turbine D. The deviation from these assumed values was due to the adjustments made in blade height necessary to correct for the effects of blade and wall cooling air by the method described in appendix H. Also, the initial assumption for axial aspect ratio for the 3100° F (1978 K) turbine D had to be multiplied by a factor of 0.90 to prevent the axial chord of the fourth blade row from decreasing below 1 inch (2.54 cm).

Cross-sectional side views of the turbines are shown in figure 14 for a visual comparison of the dimensional differences between the turbines and, as in figure 4(a) and (b), to compare them in size to the tip diameter of the compressors they drove. Hub- and tip-wall flare angle i was also determined graphically from figure 14. Only one turbine was equal in diameter to the compressor it drove. Four were larger and three were smaller. Seven of the turbines had constant mean diameters from inlet to exit. The second stage of the turbine for the quiet afterburning turbojet E required a small increase in mean diameter to satisfy simultaneously the desired inlet and exit axial critical velocity ratio, and the assumed level of exit whirl and rotor hub reaction.

The overall lengths of the turbines, as noted in figure 14, varied from 10.0 to 14.2 inches (25.4 to 36.0 cm) for the afterburning turbojets E, G, and G, and from a very short 6.8 inches (17.3 cm) to 15.6 inches (39.6 cm) for the dry turbojets D and E. In determining the overall turbine lengths, axial clearance gaps of 0.5 inch (1.27 cm) were assumed between blade rows. As noted, the longest turbines were those for the quiet engines E, and the shortest turbine was for the highest-temperature engine D. The ap-

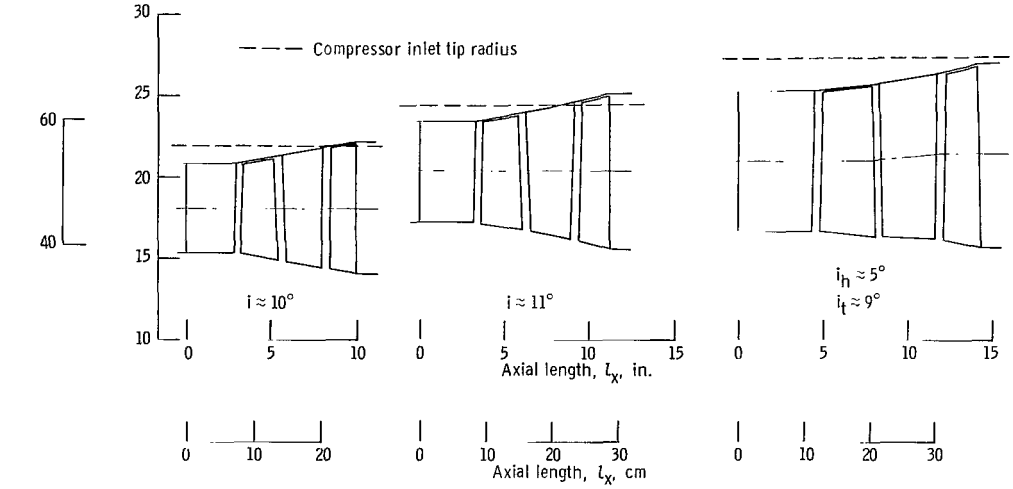

(a-1) Engine G (max. afterburning at takeoff, 122.3 PNdB).

(a-2) Engine F (no afterburning at takeoff 120.8 PNdB).

(a-3) Engine E (quiet takeoff, 116.0 PNdB).

(a) 2200° F (1478 K) afterburning turbojet engines.

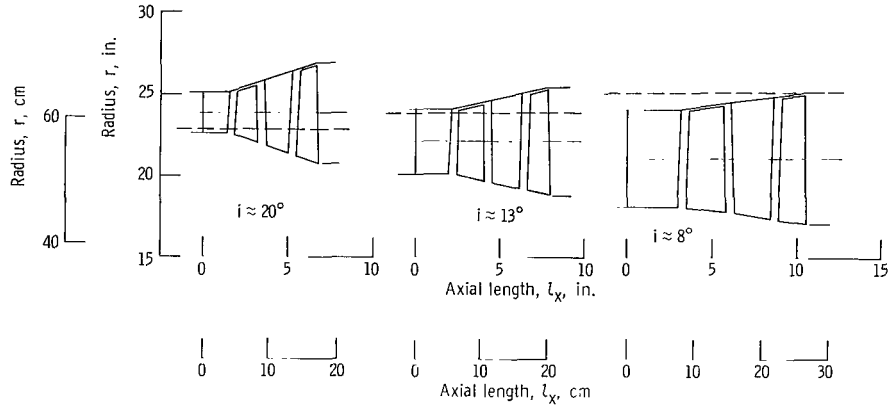

(b-1) Engine D; inlet temperature, 3100° F (1978 K).

(b-2) Engine C; inlet temperature, 2800° F (1811 K).

(c-2) Engine B; inlet temperature, 2500° F (1645 K).

(b) High-temperature dry turbojet turbines.

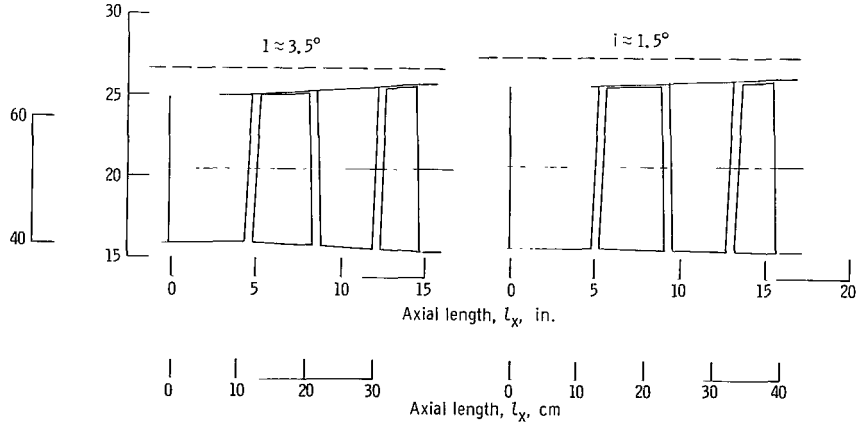

(c-1) Engine A.

(c-2) Engine E (quiet takeoff).

(c) 2200° F (1478 K) dry turbojet turbines.

Figure 14. - Profiles of turbines in radial-axial plane.

proximate values of the hub- and tip-wall flare angle i varied from a high value of approximately 20° for the 3100° F (1978 K) turbine D, required to accommodate its high total-pressure ratio of 4.6 and cooling airflow ratio of 0.30, to approximately 1.5° for the turbine for the quiet dry turbojet engine E which had a total-pressure ratio of only 2.1 and a cooling airflow ratio of only 0.067. Although the turbine for the afterburning quiet turbojet engine E had almost the same total-pressure ratio and cooling airflow ratio, its flare angle was larger (averaging 7°) because of the lower level of exit critical velocity ratio used in its design (0.45 as compared to 0.51).

The resultant effect of the aforementioned blade speeds and geometry on rotor blade centrifugal stress is shown as a function of turbine exit weight flow in figures 15(a) and (b) for the turbines for the afterburning turbojet and dry turbojet engines, respectively. The symbols identify the turbine inlet temperatures and the quiet engines. The level of stress shown is for an assumed linear taper ratio of 2:1 in blade cross-sectional area from blade hub to tip. This assumption of a constant taper ratio ignores the possible effects that variations in blade radius ratio and blade internal cooling configuration can have on taper ratio. Consideration of this effect, however, was judged to be beyond the scope of the analysis, as was the possible effect of rotor blade tip shrouds on stress.

However, trends and comparisons can be made from the curves. Second-stage rotor blade centrifugal stress was always higher than the first-stage stress because of the increase in blade height. The difference in stress between the two stages was directly related to the rate at which the blade height increased from turbine inlet to exit, and, therefore, the difference in stress increased with increasing flare angle. Just as the flare angles were less for the two low-temperature dry turbojet turbines A and E, compared to the three dry turbojet turbines B, C, and D, so was the difference in stress less between stages, as shown on the figure.

First-stage rotor stress decreased rapidly with increasing turbine inlet temperature for the dry turbojet turbines noted in figure 15(b), because of the large reduction in first-stage rotor blade radius ratio. A 2:1 reduction in first-stage rotor stress was noted in going from the turbine for the quiet dry turbojet E, to the 3100° F (1978 K) turbine D. Second-stage rotor blade stress also decreased with increasing turbine inlet temperature for the same reason, but not as rapidly, and beyond a temperature of 2800° F (1811 K) started increasing again because of the increase in blade diameter and blade speed.

The blade stress for the first- and second-stage rotors of the afterburning turbojet turbines E, F, and G, were generally lower and higher, respectively, than the corresponding 2200° F (1478 K) turbines for the dry turbojet engines A and E. The reasons are apparent when the turbines for the two quiet engines E are compared. Because both turbines were designed for the same weight flow and rotative speed, the difference in stress lies in the difference between turbine diameters and blade heights (annulus area). Referring to table II, it was noted that the somewhat higher level of axial critical veloc-

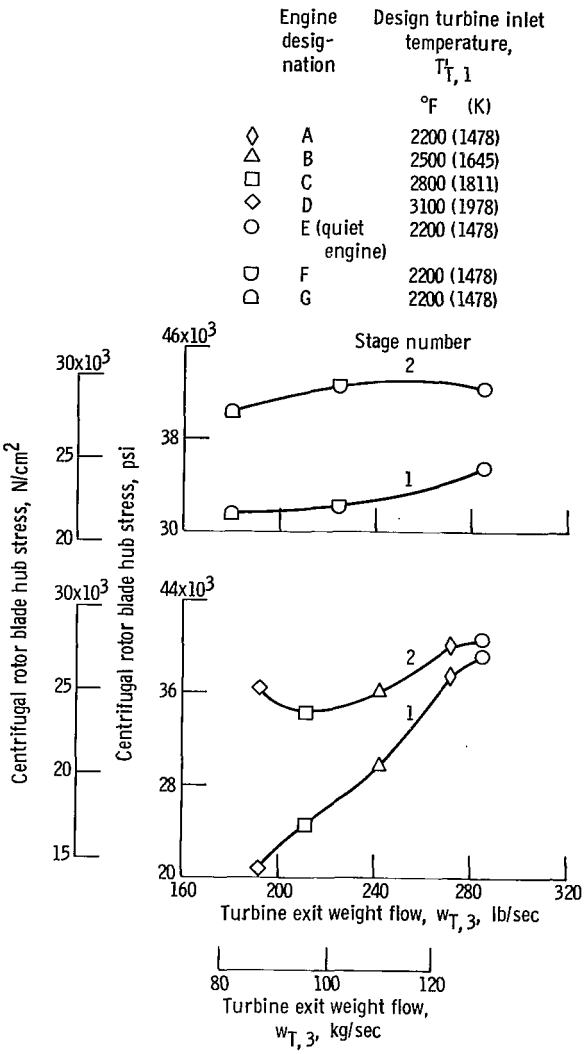

(b) Dry turbojet turbines.

Figure 15. - Effect of engine design requirements on centrifugal rotor blade hub stress at design rotational speed for blade taper ratio of 2.0. Pattern factor, 0.15; blade thermal cooling effectiveness, 0.70; cooling air temperature reduction across cooling air heat exchanger, 400° F (222 K).

ity ratio (0.28) entering the afterburning turbojet turbine E, compared to 0.24 entering the dry turbojet turbine E, resulted in a reduction in rotor inlet blade height from 10.0 to 8.6 inches (25.4 to 21.85 cm). The effect was to reduce first-stage rotor stress. However, the reverse was true at the exit of the turbines where the level of exit critical velocity ratio for the afterburning turbojet turbine was lower than for the dry turbojet turbine. The difference in exit critical velocity ratio was 0.45 compared to 0.51, respectively, requiring a larger exit annulus area for the afterburning than for the dry

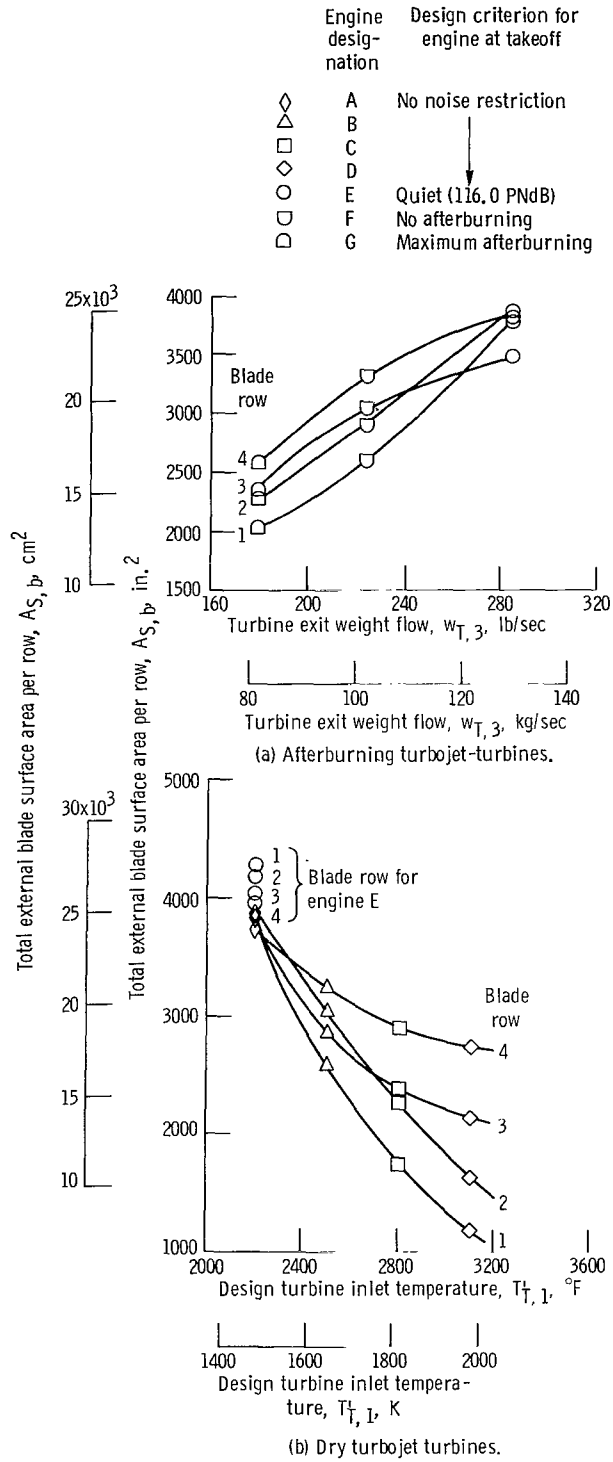

Figure 16. - Effect of engine design requirements on turbine blade external surface area. Pattern factor, 0.15; blade thermal cooling effectiveness, 0.70; cooling air temperature reduction, 400° F (222 K).

turbojet engine. In this case, however, the increase in area had to come by way of an increase in exit diameter rather than in blade height in order to maintain a constant value of hub reaction. The result was an increase in blade speed and stress.

The variation in blade stress shown in figure 15 indicates that a variation in blade life would exist between turbines and turbine stages unless a compensating adjustment in blade metal temperatures was made. However, no adjustment was made because of the corresponding variation in blade radius ratios between turbines, shown in table IV, and, as noted previously, in the possible effect of blade radius ratio on blade taper ratio.

The total external blade surface area per row for each turbine defined in appendix E as $A_{s,b}$ is shown in figures 16(a) and (b) as a function of turbine exit weight flow and turbine inlet temperature for the afterburning and dry turbojet turbines, respectively. The dimensional information contained in table IV together with the relations developed in appendix E, was used to obtain the areas. The areas, in turn, were used to determine the required heat sink Q_R necessary to cool the blading by using the relations developed in appendix F.

In general, the blade surface areas decreased with decreasing turbine exit weight flow and increasing turbine inlet temperature, and increased from rows 1 to 4. There were some exceptions, however, as will be noted. Areas for the first blade row of the three afterburning turbojet turbines (fig. 16(a)) varied approximately proportionally with turbine exit weight flow, from 2030 to 3800 square inches (13 100 to 24 500 cm^2). Surface areas for the two noisy engines F and G increased nearly linearly with blade row from rows 1 to 4 by approximately 30 percent. The area for the third row of the quiet engine E was less than the other three rows, however, because of a relatively high blade aerodynamic loading coefficiency ψ_s and, hence, a reduced solidity and reduced number of blades in the row. The blade surface areas for the remaining three blade rows were nearly identical, varying from 3800 to 3860 square inches (24 500 to 24 900 cm^2).

Blade surface areas for the five dry turbojet turbines are shown in figure 16(b). The areas generally decreased with increasing turbine inlet temperature and engine noise, particularly for the first stage, because of the corresponding decrease in engine weight flow. The increase in area with blade row number varied widely from approximately 130 percent for turbine D with the highest turbine inlet temperature, pressure ratio, and flare angle, to almost no increase in area for the lowest-temperature turbines A and E, having the smallest flare angle and, therefore, the least increase in blade height from turbine inlet to exit.

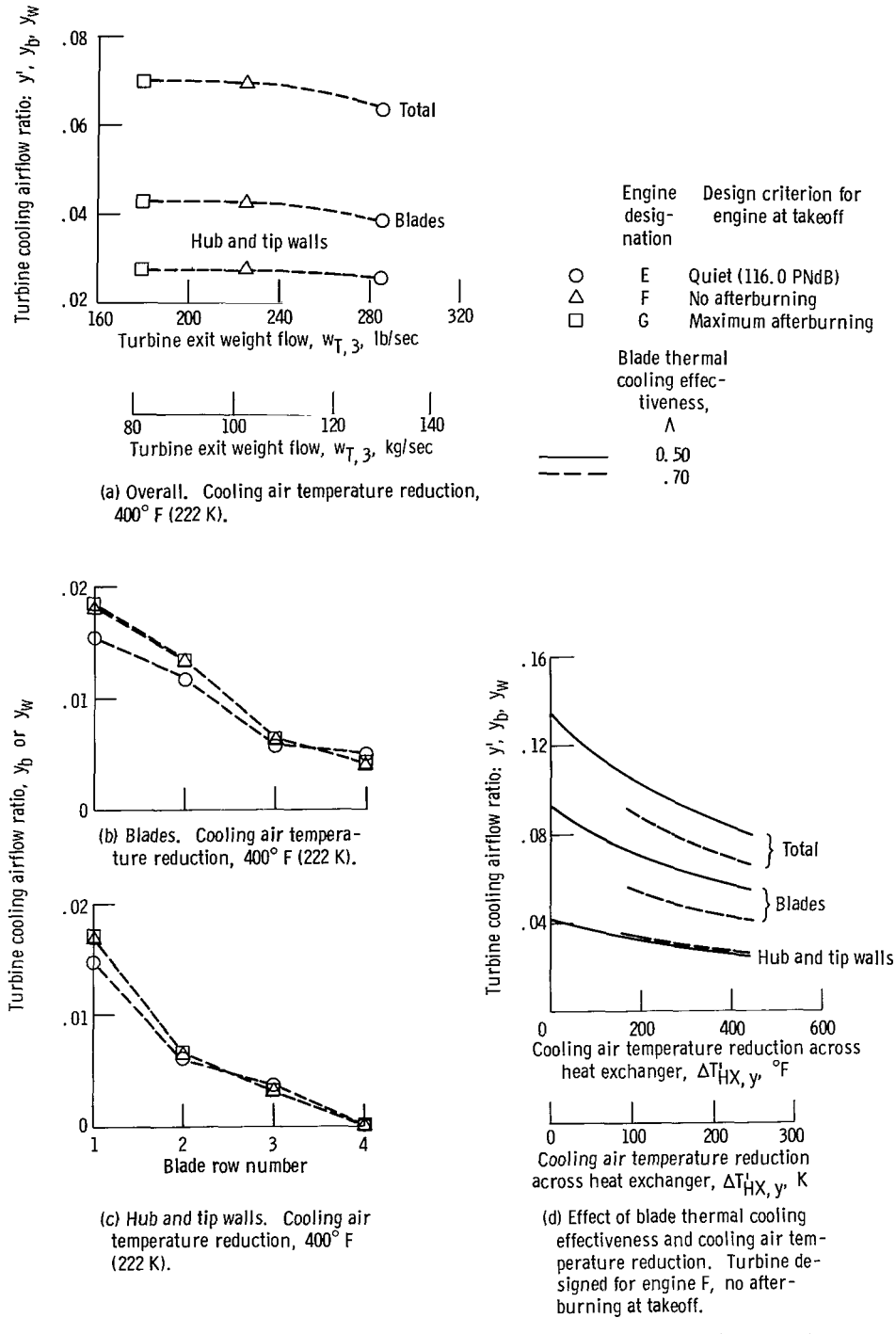

(a) Overall. Cooling air temperature reduction, 400° F (222 K).

(b) Blades. Cooling air temperature reduction, 400° F (222 K).

(c) Hub and tip walls. Cooling air temperature reduction, 400° F (222 K).

(d) Effect of blade thermal cooling effectiveness and cooling air temperature reduction. Turbine designed for engine F, no afterburning at takeoff.

Figure 17. - Effect of engine design requirements, blade thermal cooling effectivenss, and cooling air temperature reduction on turbine cooling air requirements for afterburning turbojet engines. Pattern factor, 0.15; design turbine inlet temperature, 2200° F (1478 K); average stator metal temperature, 1720° F (1211 K); average rotor metal temperature, 1620° F (1155 K); hub and tip wall metal temperature, 1600° F (1145 K).

Cooling Requirements

The total cooling airflow ratios y' required to cool the eight turbines investigated herein were presented in figure 5. In this section, there is presented a more detailed breakdown of the cooling airflow ratios required for each blade row y_b and wall y_w, together with the average blade heat-transfer coefficients $\bar{h}_g$. The methods used to determine these cooling airflow ratios, together with the blade and wall metal temperatures used to satisfy the assumed life criterion for the turbines were noted in the section TURBINE DESIGN CONSIDERATIONS and are discussed in appendixes F and G.

Afterburning turbojet turbines. - The incremental cooling airflow ratios for the three afterburning turbojet turbines E, F, and G are shown in figure 17(a). As noted, approximately 60 percent of the total coolant airflow (over 0.04) was required to cool the blading. The rest was required to cool the hub and tip walls (nearly 0.03). The figure also notes that for turbines G and F, which had equal turbine inlet temperatures, pressures, and exit critical velocity ratios, a 25 percent increase in the size (exit weight flow) of the turbine from 180 to 225 pounds per second (81.6 to 102.0 kg/sec), respectively, had essentially no effect on the cooling airflow ratio required. However, by decreasing the compressor pressure ratio from 10.0 to 8.0 for turbine E, the total cooling airflow ratio was reduced approximately 10 percent from 0.070 to 0.064, because of the reduction in the temperature of the cooling air, as noted previously, and because of the reduction in heat-transfer coefficient $\bar{h}_g$, as will be noted later.

The breakdown per blade row for the blade and wall cooling airflow ratio is shown in figures 17(b) and (c), respectively. Cooling airflow ratios for the blades and walls were nearly equal for the first blade row (stator), but the wall cooling requirements decreased more rapidly with succeeding blade rows. Essentially no wall cooling was required for the fourth row. Blade cooling airflow ratios decreased almost linearly with row number from values of 0.015 or 0.018 for the first row, to approximately 0.005 for the last row. Cooling airflow ratios were somewhat less for the first three rows of the quiet turbojet turbine E, partly because of the lower temperature of the cooling air and the reduced level of the product of velocity and density (fig. 12), and hence the reduced level of the heat-transfer coefficient $\bar{h}_g$ for these rows. However, the cooling airflow ratios for the fourth row of this turbine were slightly above those for the two noisy engines because of the lower specific work, which resulted in a higher gas temperature at the turbine exit.

The effect of blade thermal cooling effectiveness Λ and temperature drop across the cooling air heat exchanger $\Delta T'_{HX,y}$ on blade and wall cooling requirements for afterburning turbojet turbine F is shown in figure 17(d). As before, blade and wall cooling air temperatures were assumed equal. The total curves shown on the figure are repeated from figure 6(a). The following points of interest may be noted from the figure:

First, the level of the cooling airflow ratio that would be required for a present technology engine and turbine (defined in appendix F as $\Delta T'_{HX,\,y} = 0$, $\Lambda = 0.50$) for the level of metal temperatures assumed in this analysis would be 0.135. Second, at the level of Λ of 0.50, it required approximately twice the cooling air to cool the blades as the walls. Third, increasing the blade thermal cooling effectiveness Λ from 0.50 to 0.70 decreased the amount of blade cooling air by a fourth, but increased slightly the amount of cooling air required to cool the walls. The independence of y_w on Λ may be noted in the relations developed in appendix G. However, the increase in y_w with increasing Λ was due to the reduced amount of blade cooling air quenching the gas stream and, therefore, to the higher inner-stage gas stream temperatures. Hence, the total airflow required to cool the turbine was reduced by only about 15 percent. Fourth, reducing the temperature of the cooling air reduced the coolant required to both the blading and the walls. Over the range of temperature reductions considered of 400° F (222 K), the wall, blade, and total cooling airflow requirements decreased approximately 40 percent. Fifth, a reduction in the cooling air temperature of approximately 150° F (83.3 K) resulted in approximately the same reduction in total cooling airflow ratio as an increase in Λ from 0.50 to 0.70.

Dry turbojet turbines. - The incremental cooling airflow ratios for the five turbines are shown in figures 18(a) to (c). The values shown in figure 18(a) as a function of turbine inlet temperature indicate that approximately 50 percent more coolant was required to cool the blades than the walls. Over the range of turbine inlet temperatures considered from 2200° to 3100° F (1478 to 1978 K), the blade, wall, and total cooling airflow ratios increased almost $4\frac{1}{2}$ times. At the peak temperature of 3100° F (1978 K), 18.2 percent of the engine's airflow was required to cool the blading, and an additional 11.6 percent was required to cool the walls. Beyond a turbine inlet temperature of 2700° F (1757 K), a higher cooling airflow ratio was required to cool the walls than was required to cool the whole turbine at 2200° F (1478 K).

The breakdown per blade row of the blade and wall cooling airflow ratios is shown in figures 18(b) and (c), respectively. The cooling airflow ratios were nearly equal for the first row of blades and walls, but the wall cooling requirements decreased more rapidly with succeeding blade rows than did the blade cooling requirements. Essentially no wall cooling was required for the fourth row for the lower-temperature turbines A and E. Blade coolant requirements decreased almost linearly with blade row number. Stator and rotor cooling airflow ratios of 0.067 and 0.058 were required to cool the first stage of the high-temperature turbine D. As much coolant was required to cool the second-stage rotor of this turbine, as to cool the first-stage rotor of the 2500° F (1645 K) turbine B. Finally, it was noted that the coolant requirements for the noisy and quiet 2200° F (1478 K) engines A and E were identical.

In appendix F, it was noted that the gas transport properties used to compute blade

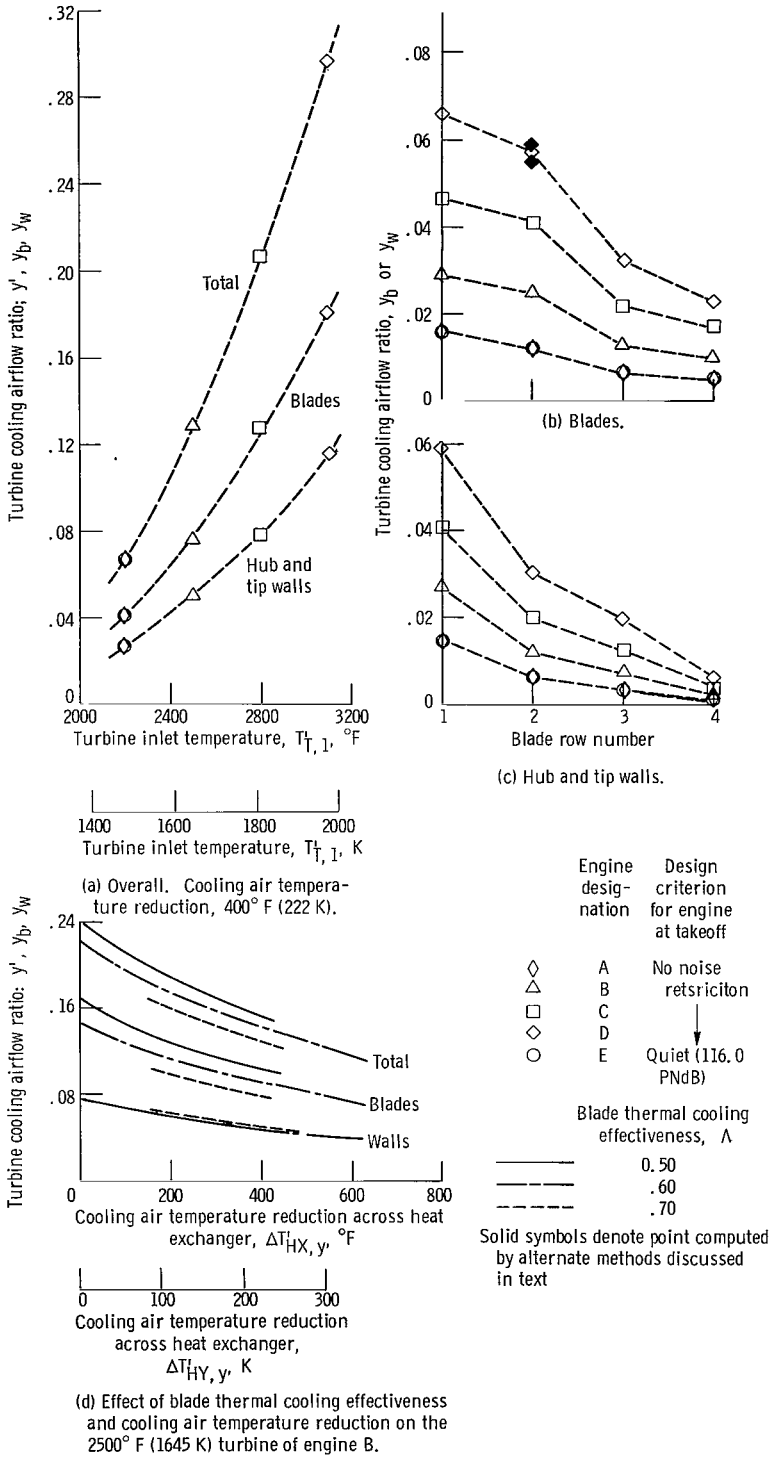

Figure 18. - Effect of engine requirements, blade thermal cooling effectiveness, and cooling air temperature reduction on turbine cooling air requirements for the dry turbojet engines. Pattern factor, 0.15; average stator metal temperature, 1720° F (1211 K); average rotor metal temperature, 1620° F (1155 K); hub and tip wall metal temperature, 1600° F (1145 K).

cooling airflow ratios were based on the average relative total temperature of the gas entering the blade row. However, alternate approaches were also considered and compared because of their more common usage in heat-transfer analysis. Herein, the transport properties are determined from either the average static temperature of the gas entering and leaving each blade row, or from the blade film temperature. In the latter case, film density is also used in place of the gas density. The effect on the resulting cooling airflow ratio for row 2 of the 3100° F (1978 K) turbine D is shown as the triple point in figure 18(b). The following ratios were obtained: 0.056 using the average static temperature of the gas, 0.058 using the total relative temperature of the gas, and 0.060 using the film temperature. Therefore, because the value obtained from the method used in this report fell in the middle, the method was considered a good compromise, and saved the complication of computing the average gas static temperature or film temperature for each blade row.

The effect on blade and wall cooling requirements of varying the assumed level of blade thermal cooling effectiveness Λ from 0.50 to 0.70, and of varying the temperature drop across the cooling air heat exchanger $\Delta T'_{HX,y}$ from 600° to 0° F (333 to 0 K) is shown in figure 18(d) for the 2500° F (1645 K) dry turbojet turbine B. The total curves shown on the figure are repeated from figure 6(b). The following points of interest may be noted from the figure: First, at a level of Λ of 0.50, approximately twice as much cooling air was required to cool the blades as the walls. Second, increasing the level of Λ from 0.50 to 0.70 decreased the amount of blade cooling air by approximately one-fourth but had essentially no effect on changing the amount of wall cooling air required. The reason for this effect was the same as noted previously for the afterburning turbojet turbine shown in figure 17(d). Therefore, the reduction in the total cooling airflow requirement for turbine B in going from a Λ of 0.50 to 0.70 was only approximately 15 percent. Third, reducing the temperature of the cooling air reduced the coolant required to both the blading and the walls. Over the first 400° F (222 K) of temperature reduction shown on figure 18(d), the wall, blade, and total cooling airflow requirements decreased approximately 37 percent from the value required if not heat exchanger were used ($\Delta T'_{HX,y} = 0$). Increasing the temperature reduction to 600° F (333 K) further decreased the cooling airflow requirements to approximately 50 percent of this value. Fourth, a reduction in the temperature of the cooling air of 150° F (83.3 K) resulted in approximately the same reduction in the total cooling airflow ratio as an increase in Λ from 0.50 to 0.70. Fifth, a total cooling airflow ratio of 0.24 would be required to cool a present technology turbine ($\Delta T'_{HX,y} = 0$, $\Lambda = 0.50$) having a turbine inlet temperature of 2500° F (1645 K), for the levels of metal temperature, compressor pressure ratio, and burner pattern factor used.

Gas-to-blade heat-transfer coefficients. - The value of $\bar{h}_g$ determined for each blade row of the eight turbines is shown in figures 19(a) and (b) as a function of turbine

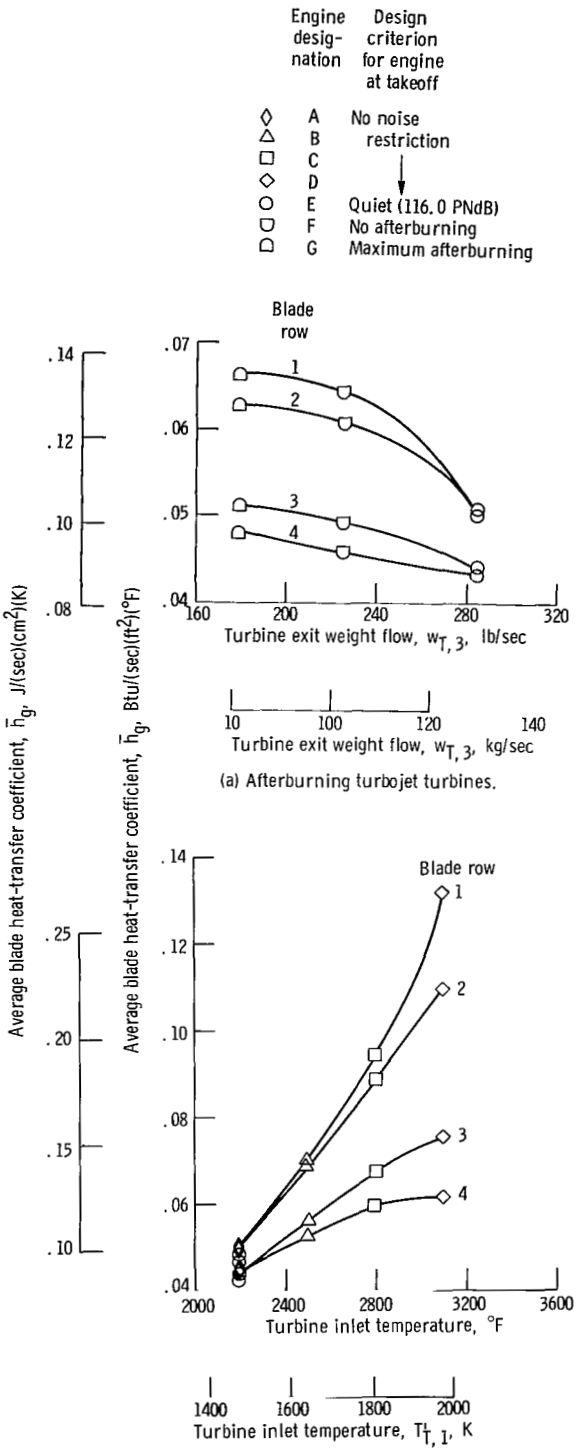

(a) Afterburning turbojet turbines.

(b) Dry turbojet turbines.

Figure 19. - Effect of engine design requirements on turbine blade heat-transfer coefficient. Pattern factor, 0.15; blade thermal cooling effectiveness, 0.70; cooling air temperature reduction across cooling air heat exchanger, 400° F (222 K).

exit weight flow and turbine inlet temperature for the afterburning turbojet and dry turbojet turbines, respectively. The values shown are the average blade external heat-transfer coefficients computed from the relations noted in appendix F, and used therein to determine the amount of heat sink required to cool the blading.

Values varied from 0.043 to 0.066 Btu per second per square foot per ^{o}F (0.008 to 0.135 J/(cm^2)(sec)(K)) for the afterburning turbojet turbines. The heat-transfer coefficients decreased with increasing turbine weight flow because of the decrease in compressor pressure ratio and, hence, in turbine inlet pressure between engines F and G and quiet engine E, and also decreased with blade row because of the decrease in gas pressure for turbine inlet to exit.

Heat-transfer coefficients varied from values of 0.043 to 0.131 Btu per second per square foot per ^{o}F (0.0879 to 0.268 J/(cm^2)(sec)(K)) for the five dry turbojet turbines shown in figure 19(b). Values for the four rows of the two 2200^{o} F (1478 K) turbines A and E were nearly identical to those shown in figure 19(a) for the quiet afterburning turbojet turbine E. From there, the values increased rapidly with turbine inlet temperature for engines B, C, and D, particularly for the first-stage blading. The increase was due primarily to the increase in the density-velocity parameter with increasing turbine inlet temperature, as noted previously in figure 13.

SUMMARY OF RESULTS

An analytical study was made of the design requirements for a series of eight turbines suitable for application to a liquid-methane-fueled turbojet-powered Mach 3 transport. Four of the designs were for dry turbojet engines having turbine inlet temperatures from 2200^{o} to 3100^{o} F (1478 to 1978 K). Two of the designs were for a 2200^{o} F (1478 K) afterburning turbojet, one sized for maximum afterburning at takeoff, and the other sized for no afterburning at takeoff. The last two turbine designs were for 2200^{o} F (1478 K) engines sized for low noise at takeoff, one for an afterburning turbojet and the other for a dry turbojet. Turbine cooling air was assumed to be bled from the exit of the compressor and cooled by passing through a methane heat exchanger before entering the turbine. Turbine blades were assumed to be convectively cooled, and hub and tip walls to be film cooled. The results of the study are summarized as follows:

1. Turbine and compressor tip diameters ranged from 44 to 54 inches (112 to 137 cm). Turbine-to-compressor tip diameter ratios were less than 1 for the quiet engines and low-temperature dry turbojet engine; equal to or close to 1 for the noisy afterburning turbojet and 2500^{o} F (1645 K) dry turbojet engines; and greater than 1 for the higher-temperature dry turbojet engines. At the highest turbine inlet temperature investigated, the turbine was 8 inches (20.4 cm) larger in diameter than its compressor.

Seven of the eight designs had a constant mean diameter from turbine inlet to exit.

2. Turbine blade heights varied from 2.5 inches (6.4 cm) for the first-stage stator of the highest-temperature dry turbojet turbine to 11.2 inches (28.4 cm) for the last-stage rotor of the quiet afterburning turbojet turbine. Corresponding values of blade radius ratio varied from 0.90 to 0.59. Blade axial chord lengths varied from 1.10 to 5.13 inches (2.8 to 13.0 cm). The design compressor pressure ratios for the engines were 19.0 and 8.0, respectively, and corrected weight flows were 386 to 553 pounds per second (175 and 251 kg/sec), respectively.

3. Turbine design pressure ratios ranged from a low value of 2.1 for the quiet engines to a peak of 4.6 for the highest-temperature turbine. Resultant hub and tip flare angles ranged from 1.5° to 20°. Values of the turbine work-speed parameter E ranged from 2.84 to 3.85. Two-stage turbines adequately covered this range of work.

4. All blade exit critical velocity ratios at the mean radius were below sonic, except one. The ratios generally increased with increasing turbine inlet temperature, increasing to a value of 1.05 at the exit of the first-stage stator of the highest-temperature turbine investigated. First-stage stator exit angles ranged from 21° to 29° from tangential.

5. The number of blades required for any one blade row exceeded 100 in the second-stage rotor of the 2500° F (1645 K) turbine, and exceeded 200 in the same blade row of the 3100° F (1978 K) turbine. Corresponding values of blade axial solidity were 1.39 and 1.53 (the maximum value obtained for any blade row).

6. The amount of blade surface area exposed to the hot gas stream decreased rapidly with increasing turbine inlet temperature because of the increasing compressor pressure ratios and decreasing weight flows, particularly for the first-stage blading. The level of first-stage rotor blade centrifugal stress also decreased with increasing turbine inlet temperature, decreasing by approximately 50 percent over the range of turbine inlet temperature considered.

7. Turbine cooling airflow ratios ranged from values of 0.064 to 0.070 for the five 2200° F (1478 K) turbines, to 0.13, 0.21, and 0.30 for the 2500°, 2800°, and 3100° F (1645, 1811, and 1978 K) turbines. These ratios were required to achieve a 1000-hour blade life, based on the stress-rupture, cyclic, creep, and oxidation properties of alloys and coatings currently available. Convection cooled blading having a blade thermal cooling effectiveness of 0.70, film-cooled hub and tip walls, a 400° F (222 K) reduction in the temperature of the cooling air, and a pattern factor of 0.15 was assumed.

8. Approximately twice as much cooling air was required to cool the convection-cooled blades having a blade thermal cooling effectiveness of 0.50 as to cool the film-cooled hub and tip walls. Increasing the blade thermal cooling effectiveness to 0.70 reduced the amount of blade cooling air by one-fourth, but had essentially no effect on the quantity of wall cooling air required.

9. When compressor pressure ratio, turbine inlet temperature, and turbine exit critical velocity ratio were held constant, a 25 percent difference in turbine size and weight flow between the two turbines designed for the noisy afterburning turbojet engines had essentially no effect on turbine blade radius ratios and axial aspect ratios, or on the amount of cooling airflow ratio required to cool the blades or the hub and tip walls.

10. When turbine inlet temperature and exit critical velocity ratio were held constant, an increase in compressor pressure ratio from 8.0 to 10.0 between the quiet and noisy afterburning turbojet engines resulted in an increase in the hub- and tip-wall flare angles from approximately 7° to 11°. There was also an increase of 10 percent in the cooling airflow ratio required to cool the turbines (from 0.064 to 0.070) for values of blade thermal cooling effectiveness and cooling air temperature reduction of 0.70 and 400° F (222 K), respectively. The increase in the cooling airflow ratio was due to increases in the temperature of the cooling air and in the gas-to-blade heat-transfer coefficients.

11. Reducing the temperature of the cooling air 400° F (222 K) reduced the amount of coolant required for both the walls and blades by 37 to 40 percent. A reduction in cooling air temperature of 150° F (83.3 K) was approximately equivalent to an increase in the blade thermal cooling effectiveness of 40 percent (from 0.50 to 0.70).

12. Turbine exit pressures did not vary appreciably between the eight turbines investigated, even though compressor pressure ratios varied from 8.0 to 19.0. A small peak in exit pressure occurred at a turbine inlet temperature of 2800° F (1811 K).

13. Turbine exit temperatures varied somewhat with turbine inlet temperature, but over a much smaller range and at a reduced level of temperature from the values used in the studies of references 1 and 2 in which engine size and aircraft payload and range capability for the mission were determined. There was essentially no increase in turbine exit temperature beyond an inlet temperature of 2500° F (1645 K), indicating little advantage in going beyond this temperature for the dry turbojet cycles at the level of compressor pressure ratios, turbine metal temperatures, and cooling methods considered herein.

14. The reduction in turbine exit temperature relative to the values used in the analyses of references 1 and 2 was caused by the reduced temperature of the cooling air (achieved in a cooling-air-to-methane heat exchanger). Another cause was the increase in the cooling airflow ratios required to cool the turbines, particularly for the three higher temperature turbines investigated.

CONCLUDING REMARKS

The results and conclusions obtained in this analysis were largely dependent on the

assumptions made, which included such important considerations as the type of engines used, the compressor pressure ratios used, the turbine blade and wall metal temperatures and cooling method used (convection-cooled blades, film-cooled hub and tip walls), the source of the cooling air, the assumed radial and circumferential turbine gas temperature profiles used, the interactions assumed between the turbine cooling air and the main gas stream, and the particular aerodynamic and geometric approach used in the design of the turbines. Conceivably, the results could have been considerably different for lower-pressure-ratio turbojet engines; for fan engines where much of the thrust is derived from the fan stream and not from just the turbine exhaust; and for more effective methods of blade cooling such as film cooling, transpiration cooling, or regenerative cooling, which may have a less severe effect on the thermodynamic performance of the turbine.

Lewis Research Center,
National Aeronautics and Space Administration,
Cleveland, Ohio, April 20, 1970,
720-03.

APPENDIX A

SYMBOLS

A	area per blade row, or area
AR	blade aspect ratio, BH/C
B	slot height
BH	blade height, fig. 23
C	blade chord length, fig. 23
C_L	blade mean camber length, fig. 23
C_P	specific heat at constant pressure
D	diameter
E	turbine work-speed parameter, $(gJ\ \Delta h/U_m^2)_T$
f/a	fuel-air ratio
g	gravitational constant
h_g	gas-to-blade heat-transfer coefficient
Δh	specific work
i	flare angle, hub or tip wall
J	mechanical equivalent of heat
k	thermal conductivity
l	length
n	number of blades
PF	pattern factor, eq. (30)
Pr	Prandtl number
p	pressure
Q	heat sink
R	gas constant
$\mathscr{R}$	reaction, $(W_2/W_1)^2$
Re	Reynolds number
r	radius
s	blade spacing, fig. 23
T	absolute temperature
t	blade thickness, fig. 23
U	blade speed
V	absolute velocity
V_{cr}	critical velocity, $\sqrt{\frac{2\gamma}{\gamma+1} gRT'}$
W	relative velocity
w	weight flow
x	effective film-cooled wall length
y	cooling airflow ratio, $w_y/w_{C,1}$
α	injection angle between wall cooling air and gas stream, or angle of relative velocity from axial
β	angle of relative velocity from tangential, fig. 23
γ	ratio of specific heats
Δ	average fraction of turbine circumference blocked by blading
δ	total pressure, ratioed to standard pressure, p'/p_{std}
ϵ	gamma correction factor, $\frac{0.740}{\gamma}\left(\frac{\gamma+1}{2}\right)^{\gamma/(\gamma-1)}$
η	efficiency based on total-to-total pressure ratio, p_2'/p_1'

$\sqrt{\theta}$ critical velocities, ratioed to standard air, $V_{cr}/V_{cr, std}$

Λ blade thermal cooling effectiveness, eq. (33)

λ film cooling effectiveness, eq. (41)

μ absolute (dynamic) viscosity

ρ density

φ blade camber angle, fig. 23

χ parameter defined in eq. (37)

ψ aerodynamic (tangential) blade loading coefficient, ref. 7

σ blade solidity, C/s

Subscripts:

A available

a annulus

ad adiabatic

B primary burner

b blade (stator or rotor)

C compressor

cr critical, corresponding to conditions at Mach 1

e engine

F fuel

f flow

g gas

HX turbine cooling air heat exchanger

h hub radius or diameter

i engine inlet

j integer

M metal

m mean radius or diameter

max maximum

R required

r rotor

S surface

s stator

std standard sea-level conditions

T turbine

t tip radius or diameter

u tangential direction

w blade platform or hub and tip wall

x axial direction

y turbine cooling air or blade coolant passage

z Zweifel, ref. 7

Stations:

1 inlet

2 exit

3 exit, after mixing with wall cooling air

I first blade row, turbine

II second blade row, turbine

III third blade row, turbine

IV fourth blade row, turbine

Superscripts:

' total or total state condition

'' total state condition relative to blading or walls

$\bar{}$ average value

APPENDIX B

NUMBER OF TURBINE STAGES

The number of stages required for each turbine was determined from a cursory study made of its specific work and blade speed requirements. Turbine specific work was determined from the general power equation which equates compressor and turbine work

$$(w\ \Delta h)_C = (w\ \Delta h)_T \tag{1}$$

(The symbols are defined in appendix A.) Then, the simplifying assumption was made that the turbine cooling air did not contribute to the specific work output of the turbine, or to the flow available for doing work. The effect of cooling air on work was neglected only for the purpose of determining the number of turbine stages. Cooling-air work was considered, however, in determining the velocity diagram requirements for the turbines, as will be shown in the following two appendixes. Equation (1) then becomes

$$\Delta h_T = \left(\frac{w_C}{w_B}\right)\Delta h_C \tag{2}$$

where

$$\Delta h_C = C_P\left(\frac{T_1'}{\eta}\right)_C\left[\left(\frac{p_2'}{p_1'}\right)_C^{(\gamma-1)/\gamma} - 1\right] \tag{3}$$

A flow model of this assumption is shown in figure 20. Noting that

$$w_B = w_{T,1} = w_C + w_F - w_y \tag{4}$$

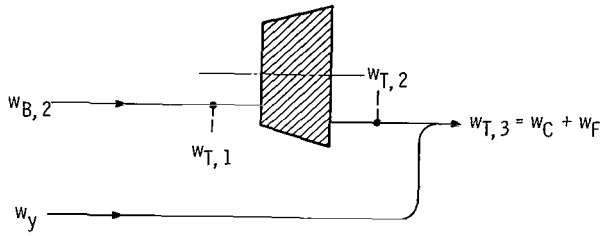

Figure 20. - Flow model used to determine number of turbine stages.

and

$$w_y = yw_C \tag{5}$$

and

$$w_F = w_C\left(\frac{f}{a}\right)_B (1 - y) \tag{6}$$

equation (1) becomes

$$\Delta h_T = \frac{\Delta h_C}{(1 - y)\left[1 + \left(\frac{f}{a}\right)_B\right]} \tag{7}$$

The values for the compressor parameters noted in equation (3), and turbine cooling airflow ratio noted in equation (7), were obtained from table I for both the design takeoff and Mach 3 cruise conditions of the engines for each of the eight turbines investigates. Values of burner fuel-air ratio consistent with the level of compressor exit and turbine inlet temperatures for each engine, and a nominal level of fuel temperature, were used.

The turbine work-speed parameter E was then determined by using the relation for E noted in appendix A and by assuming an equivalent blade speed $(U_m/\sqrt{\theta_1})_T$ of 500 feet per second (152 m/sec) for each turbine. The resulting values of the work-speed parameter are shown in figures 21(a) and (b). The wide variation in E between turbines is evident, particularly at the cruise condition. For example, the value for the 3100° F (1978 K) dry turbojet turbine (engine D) is 3.66, which is approximately 60 percent greater than the value of 2.31 required for the turbine of either low-noise engine at cruise (engine E).

Selecting the proper number of stages to deliver this work is a compromise between several factors, including turbine efficiency, size, weight, stress, and cooling considerations. Performance evaluations of one-, two-, and three-stage turbines have shown that for the range in the work-speed parameter (fig. 21(b)), levels of turbine efficiency consistent with the constant value of 88 percent assumed in the analyses of references 1 and 2 can be achieved with two-stage turbines. The performance of one such turbine is reported in reference 4, showing this capability in specific work, speed, and efficiency.

However, the turbines required for dry turbojet engines E and D operated at levels of specific work and speed where single- and three-stage turbines, respectively, could also be considered. In turbine E, as an example, the maximum value of the work-speed

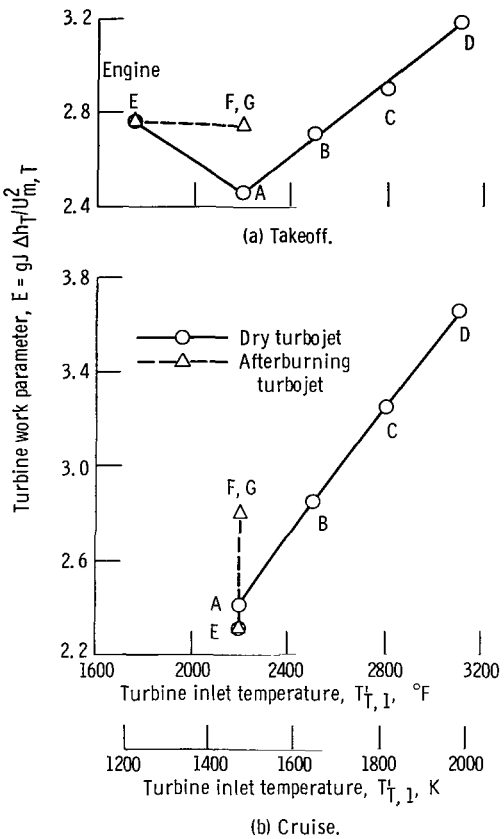

Figure 21. - Effect of engine type, operating condition, and turbine inlet temperature on turbine work-speed parameter (assuming equivalent mean blade speed of 500 ft/sec (152 m/sec), and turbine specific work computed from eq. (7)).

parameter (2.31) comes close to matching the capabilities of the highly loaded single-stage turbine reported in reference 5. Also, the performance characteristics of a three-stage turbine reported in reference 6 showed that the high level of the work-speed parameter (3.66) required for the turbine of engine D could be met more easily with a three-stage than with a two-stage turbine. However, the larger diameters and higher discharge velocities of a single-stage turbine could have detrimental effects on the overall design and performance of the engine. Also, with the large quantity of cooling air required for cooling the high-temperature turbine of engine D, a reduction in turbine equivalent specific work would be expected if the more realistic assumption was made that its cooling air contributed to the work output of the turbine. Therefore, for these reasons, only two-stage turbines were considered for the applications investigated in this report.

APPENDIX C

TURBINE SPECIFIC WORK

To account for the effects of turbine cooling air on turbine specific work, equation (1) was expanded to the form

$$(w\ \Delta h)_C = w_B\ \Delta h_T + (w\ \Delta h)_y \tag{8}$$

For purposes of the analysis, it was assumed that the cooling air used for turbine blade cooling produced one-half the equivalent specific work of the main gas stream

$$\left(\frac{\Delta h}{\theta}\right)_{y,b} = \frac{1}{2}\left(\frac{\Delta h}{\theta}\right)_T \tag{9}$$

or, in the approximate form as used herein,

$$\left(\frac{\Delta h}{T'}\right)_{y,b} = \frac{1}{2}\left(\frac{\Delta h}{T'_1}\right)_T \tag{10}$$

It was further assumed that the cooling air required to cool the blade hub and tip walls did no work. A flow model noting these assumptions is shown in figure 22.

By combining equations (8) and (10) and multiplying and dividing through by temperature, an expression for turbine specific work was obtained which was a function of the weight flow and specific work of the compressor, the weight flow of the gas entering the turbine, the blade cooling airflow ratio, and the temperature ratio between the cooling

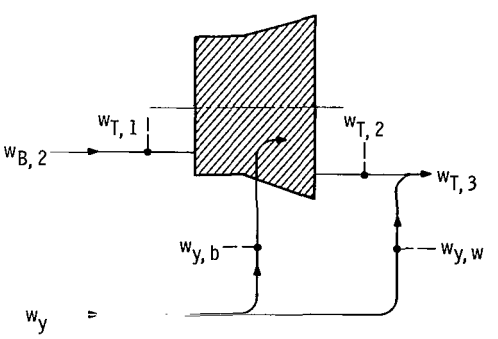

Figure 22. - Flow model used to determine turbine specific work (eq. (14)).

air and gas flow entering the turbine, as follows:

$$(w\ \Delta h)_C = (w_B T'_{T,1})\left(\frac{\Delta h}{T'_1}\right)_T + (w_b T')_y \left(\frac{\Delta h}{T'}\right)_{y,b} \tag{11}$$

$$(w\ \Delta h)_C = (wT')_{T,1}\left(\frac{\Delta h}{T'_1}\right)_T + \frac{(w_b T')_y}{2}\left(\frac{\Delta h}{T'_1}\right)_T \tag{12}$$

or

$$\Delta h_T = \frac{(w\ \Delta h)_C}{w_{T,1} + \frac{w_{y,b}}{2}\left(\frac{T'_y}{T'_{T,1}}\right)} \tag{13}$$

Then, substituting equations (4) to (6) into equation (13), and rewriting yields

$$\Delta h_T = \frac{\Delta h_C}{\left\{(1-y)\left[1+\left(\frac{f}{a}\right)_B\right]\right\}\left(1+\frac{1}{2}\left\{\frac{y_b}{(1-y)\left[1+\left(\frac{f}{a}\right)_B\right]}\right\}\frac{T'_y}{T'_{T,1}}\right)} \tag{14}$$

Equation (14) was then used in conjunction with the following equation for tangential momentum to determine the tangential vectors of the velocity diagrams for the various turbines investigated.

$$\Delta V_{u,m} = \frac{gJ(\Delta h)_T}{U_m} \tag{15}$$

APPENDIX D

TURBINE VELOCITY DIAGRAMS

Hub, mean, and tip velocity diagrams were computed from the values of turbine takeoff weight flow, rotational speed, and cruise specific work discussed previously. From these values, the flow velocities and angles, blade heights, blade diameters and blade angles, and inner-stage pressures and temperatures were determined for the eight turbines for engines A to G.

The following assumptions which were made to specify the velocity diagrams are generally consistent with present day design practice:

(1) Free-vortex distribution of the flow from blade hub to tip between each blade row, using the equations for simplified radial equilibrium: V_x = Constant, rV_u = Constant

(2) Power split between stages of 56 and 44 percent

(3) Constant mean blade diameter D_m rotor inlet to rotor exit

(4) Turbine exit leaving angle of -5^o from axial

(5) Accelerations in velocity of 11 and 8 percent across the hubs of the first- and second-state rotors, corresponding to values of $\mathscr{R}_{h,r} = (W_2/W_1)^2_{T,h,r}$ of 1.22 and 1.16, respectively.

(6) Overall turbine efficiency varying linearly from 90 to 87 percent from turbine inlet temperatures of 2200^o to 3100^o F (1478 to 1978 K), respectively

This reduction in overall efficiency was assumed to account for the effect of increased momentum losses in the main gas stream as a result of increases in the cooling airflow ratio and work-speed parameter E with increasing turbine inlet temperature. Therefore, the efficiencies are in variance with the constant value of 88 percent assumed in references 1 and 2.

(7) First-stage turbine efficiency 1 point below the overall efficiency

(8) First-stage stator total-pressure loss of 3 percent

(9) No flare in either the hub or tip walls across the first-stage stator (straight walls)

The assumptions and requirements in items (1) to (9) were then programmed on a high-speed digital computer, and all possible solutions were computed over an arbitrary range of turbine exit radius ratio and tip diameter. The solution that best met the additional criteria noted in the following items was then selected as the final design for each turbine.

(10) A turbine exit tip diameter as close to equaling that of the compressor inlet tip diameter as possible

(11) Turbine exit axial critical velocity ratio $(V_x/V_{cr})_{T,2}$ as close to 0.45 and 0.50 as possible for the afterburning and dry turbojet engines, respectively

(12) Inner-stage axial critical velocity ratios V_x/V_{cr} that smoothly accelerate to the design exit value of 0.45 or 0.50

(13) Blade hub and tip walls that flare smoothly from first-stage stator exit to turbine exit

(14) No critical velocity ratios $(V/V_{cr})_m$ or $(W/W_{cr})_m$ greater than 1

(15) No second-stage stator tip reactions $(V_2/V_1)^2_{t,III}$ less than 1

Although the overall engine and turbine requirements for the quiet engine E were the same whether it was a dry turbojet or an afterburning turbojet (see table I), the turbine geometries differed in order to satisfy the requirement of assumption (11). Therefore, a total of eight turbines were designed in this report, five turbines for the dry turbojet engines covering a range of turbine inlet temperatures and takeoff jet noise, and three turbines for the afterburning turbojet engines covering a range of takeoff jet noise.

One of the objectives of the analysis was to determine more exactly the values for the terms that go into computing the cooling airflow ratios required to cool the turbine. The procedure used to determine these ratios is discussed in appendixes F and G. However, because cooling a turbine with compressor discharge air is more critical at high flight Mach numbers than at takeoff, all the turbine design conditions computed in this and subsequent appendixes are computed at cruise conditions: That is, at cruise values of equivalent turbine specific work.

The state properties of the gas used in the design of the turbines were the computed products of burning a fuel containing 93.5 percent by weight of liquid methane (CH_4), 1.6 percent by weight of liquid nitrogen (N_2), and 4.9 percent by weight of various hydrocarbons and carbon dioxide (CO_2), with air. The computed property values are given in table V. Average property values of $\bar{\gamma}$ and $\bar{C}_P$ were used to compute stage temperatures and pressure ratios across the turbine by using the following equations:

$$(T'_1 - T'_2)_{T,\,stage} = \left(\frac{\Delta h_{stage}}{\bar{C}_P}\right)_T \tag{16}$$

$$\left(\frac{p'_2}{p'_1}\right)_{T,\,stage} = \left(1 - \frac{\Delta h}{\bar{C}_P T'_1 \eta}\right)^{\bar{\gamma}/(\bar{\gamma}-1)}_{T,\,stage} \tag{17}$$

TABLE V. - TURBINE GAS STATE PROPERTIES

Engine designation[a]	Turbine inlet temperature, $T'_{T,1}$		Gas constant, R		Specific-heat ratio		Average turbine specific heat at constant pressure, $\bar{C}_{P,T}$	
			ft-lb/(lb)(^{O}R)	J/(kg)(K)	At turbine inlet, $\gamma_{T,1}$	Average for turbine, $\bar{\gamma}_T$	Btu/(lb)(^{O}R)	J/(g)(K)
	^{O}F	K						
A	2200	1478	54.00	290.7	1.293	1.299	0.301	1.260
B	2500	1645	54.15	291.3	1.281	1.289	.310	1.297
C	2800	1811	54.23	292.0	1.269	1.280	.320	1.340
D	3100	1978	54.46	293.1	1.254	1.268	.334	1.398
E	2200	1478	54.01	290.8	1.293	1.298	.301	1.260
F, G	2200	1478	53.98	290.5	1.294	1.301	.300	1.255

[a]See table I for details.

Relative total temperatures T''_g were determined by using the relation

$$T'' - T' = \frac{W^2 - V^2}{2gJ\bar{C}_P} \tag{18}$$

Gas properties varied as a function of turbine inlet temperature and fuel-air ratio. The fuel-air ratio, in turn, was a function of the lower heating value of the fuel and the temperature of the fuel and air entering the burner. Although the fuel was assumed to be stored as a liquid on board the aircraft at or below its boiling temperature of -259^{O} F (112 K), it was assumed for purposes of determining the turbine gas properties and turbine inlet weight flow that the fuel entered the primary burner as a gas at a temperature of 77^{O} F (298 K).

The selection of 77^{O} F (298 K) was arbitrary. Fuel temperatures as high as 1300^{O} to 1400^{O} F (978 to 1033 K) are possible with the engine configuration noted in figure 3 for the highest-temperature turbine considered (engine D). However, a large variation in fuel temperature, indicative of using either more or less of the heat-sink capacity of the fuel before it enters the primary burner, did not have a large effect on either the gas properties or the total flow entering the turbine. As an example, an increase in the temperature of the gaseous fuel entering the burner from 77^{O} to 1000^{O} F (298 to 811 K) increases the sensible heat of the fuel by approximately 730 Btu per pound (1700 J/g). Compared to the heating value of 21 200 Btu per pound (49 300 J/g) noted in ref-

erences 1 and 2 for methane fuel, this results in a decrease in the required fuel-air ratio of 3.4 percent. Such a decrease would have essentially no effect on the gas properties, only a 0.05 to 0.09 percent reduction in turbine weight flow, but would possibly have a significant effect on reducing engine specific fuel consumption. This latter effects, however, was not relevant to the criteria necessary for the design of the turbines.

APPENDIX E

TURBINE BLADE GEOMETRY

A method was developed to determine the approximate blade configuration required for each blade row of each turbine investigated. The objective was to determine blade configurations which would be capable of good aerodynamic performance, but into which reasonable blade air-cooling schemes could be incorporated. The method consisted of surveying several existing turbine stator and rotor blade configurations covering a range of blade turning angles and leaving angles. From the survey, a series of working curves were made which related blade mean-camber length C_L, axial chord length C_x, gas entering and leaving angle β_1 and β_2, camber angle φ, and axial solidity σ_x. (Symbols are defined in appendix A and in fig. 23.) Values of blade aerodynamic (tangential) loading coefficient ψ, and aspect ratio AR, consistent with those used in current turbine designs were used to determine blade axial solidities σ_x and axial chord lengths C_x for each blade row. The curves were then used to obtain the dimensional characteristics of the blading required for the various turbines investigated by interpreting the curves at the mean-radius values of gas entering and leaving angles computed in appendix D.

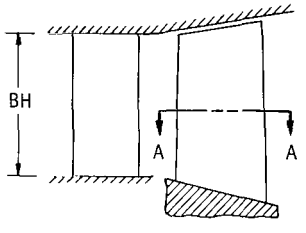

(a) Profile view of stage in radial-axial plane.

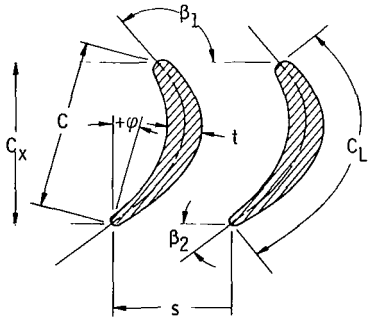

(b) Section A-A.

Figure 23. - Blade geometry symbols. Aspect ratio (axial), $AR_x = BH/C_x$; solidity (axial), $\sigma_x = C_x/s$; turning, $\Delta\beta = \beta_1 - \beta_2$.

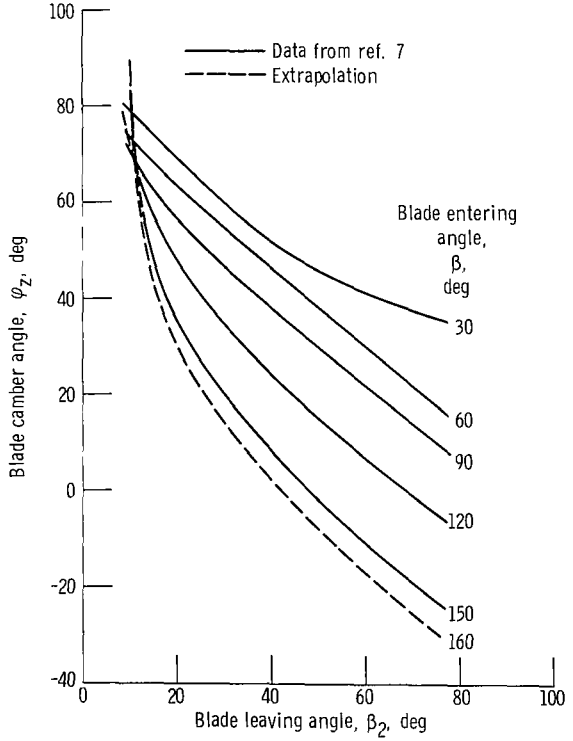

Figure 24. - Variation of turbine blade camber angle with blade entering and leaving angles.

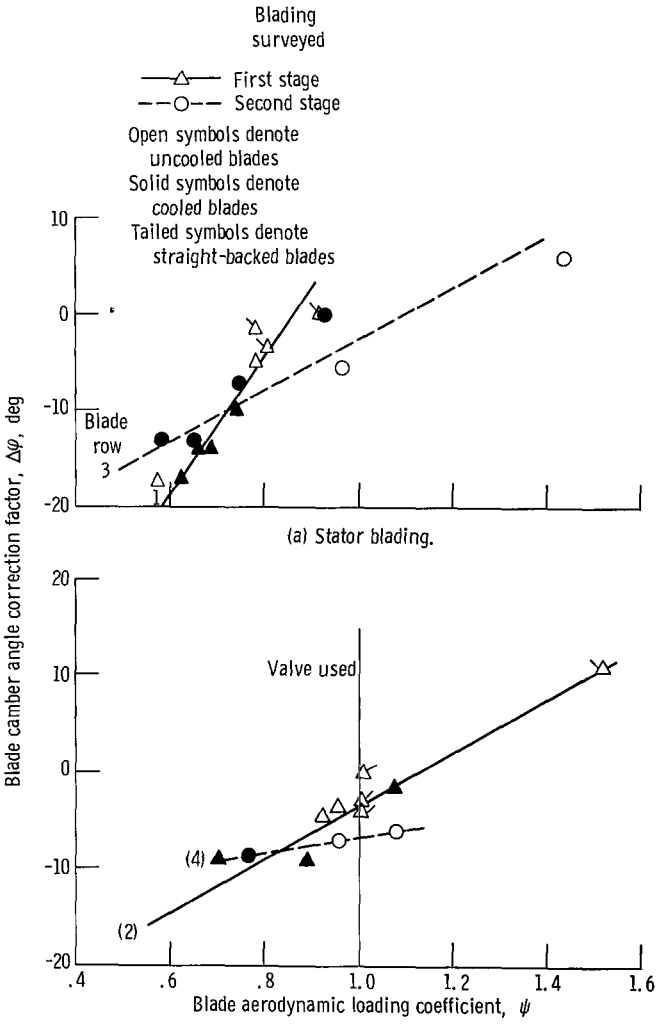

Figure 25. - Effect of turbine blade loading coefficient on blade camber angle ($\varphi = \varphi_z + \Delta\varphi$).

The remainder of this appendix elaborates on the development of the work curves (figs. 24 to 28) and procedure just mentioned. The first curve (fig. 24) was constructed from information contained in reference 7, and relates blade camber angle φ_z, with blade entering and leaving angle β_1 and β_2. The results of the survey of a compilation of existing turbine blade profile data was used to check the validity of figure 24. In so doing, it was found that blade camber angle was also influenced by the aerodynamic loading coefficient ψ, and by the particular blade row for which the blading was designed. The effect is shown in figure 25 which relates ψ to a correction factor $\Delta\varphi$ for each of the four blade rows. The actual blade camber angle φ for the blading surveyed was therefore equal to

$$\varphi = \varphi_z + \Delta\varphi \tag{19}$$

where

$$\varphi_z = f(\beta_1,\ \beta_2,\ \text{and fig. 24})$$

and

$$\Delta\varphi = f(\psi,\ \text{blade row number (fig. 25)})$$

The points plotted on figure 25 are of the various blade configurations considered in the survey. They included cooled, uncooled, straight-backed, and curved-back blading for one- and two-stage turbines. It may be seen from the figure that the points roughly defined a linear relation between $\Delta\varphi$ and ψ, differing in slope and magnitude for each blade row. The slopes were higher for first-stage blading than for second stage, and higher for stators than for rotors. Therefore, the first-stage stators were the most affected, requiring the largest correction in blade camber angle with changes in tangential loading coefficient. The second-stage rotor blading required the least correction. As before, no difference in these trends could be observed between cooled, uncooled, curved-back, or straight-back blading.

In order to use figure 25, the aerodynamic loading coefficient ψ had to be known or assumed for each blade row. In analyzing the design characteristics of the stator blading surveyed, a general relation was found between the blade leaving angle β_2 and ψ. This relation is shown in figure 26 for the first- and second-stage stator blading considered in the survey. With few exceptions, the points defined approximately a linear relation between the two parameters. The line drawn through the points was therefore used to determine the stator loading coefficients and, in conjunction with figure 25, the correction factor $\Delta\varphi_s$ for the stator blade camber angle.

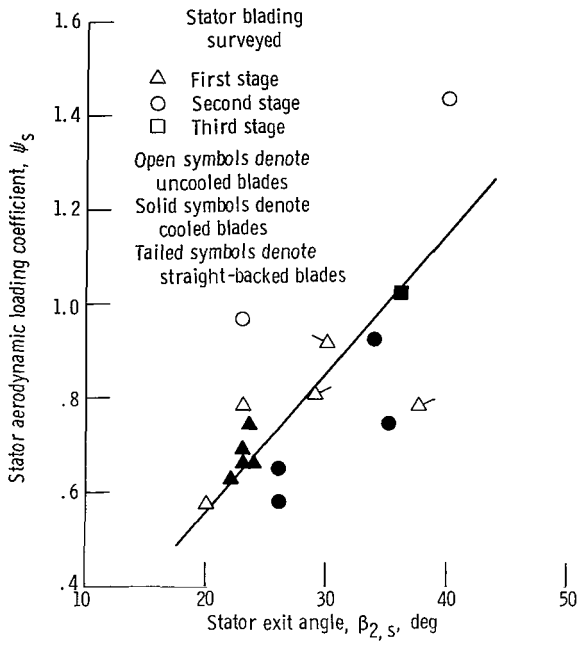

Figure 26. - Variation of turbine stator aerodynamic loading coefficient with exit angle.

No similarly meaningful relation was found for the rotor blading surveyed. However, it was noted that a majority of the more recent rotor blade designs developed for high performance engines had values of ψ ranging between 0.9 and 1.1. Therefore, a value of 1.0 was assumed and used. With this assumption, figure 25 then indicated that the correction factor for camber angle $\Delta\varphi_r$ would be a constant -3.5° and -6.5°, respectively, for all first- and second-stage rotor blading.

Blade axial chord lengths were determined by dividing the blade heights found in appendix D by their aspect ratio

$$C_x = \frac{BH}{AR_x} \tag{20}$$

The values used for AR_x were assumed to be the average of the values obtained from the blading surveyed. Only the cooled blading of curved-backed design was included from the survey because of the high-temperature, highly stressed nature of the turbines required for the applications in this report. By so doing, the values for AR_x rounded off to the nearest 0.5, were found to be 2.0, 3.0, 3.0, and 5.0, respectively, for the four blade rows. In cases where these values of AR_x resulted in an axial chord length C_x of less than 1 inch (2.54 cm) for any of the blade rows, the values of AR_x for all the rows were multiplied by a factor of 0.9, 0.8, etc., until the minimum value of C_x ex-

ceeded 1 inch (2.54 cm). This was done to assure that the cross-sectional area of the various blade profiles would be large enough to accommodate internal cooling air passages.

The next group of curves (figs. 27 and 28) were developed to obtain the blade mean camber lengths C_L, and blade surface areas A_b needed in appendix F to compute the blade cooling airflow requirements. Figure 27 was developed from information contained in reference 7, and relates blade camber angle φ, axial chord C_x, and blade turning $\beta_2 - \beta_1$ to mean camber length C_L. The latter two terms are expressed as $\Delta\beta$ and the ratio $(C_L/C_x)_z$. The corresponding parameters for the survey blading mentioned previously were then checked against figure 27 to determine the validity of the plot. In so doing, it was found that a relation existed between the blade thickness ratio t_{max}/C_L and the ratio $(C_L/C_x)_z$ for the first stage stator blading. This relation is shown in figure 28 as the factor by which $(C_L/C_x)_z$ had to be multiplied to get the measured values of C_L/C_x for the blading surveyed. The points on the figure defined ap-

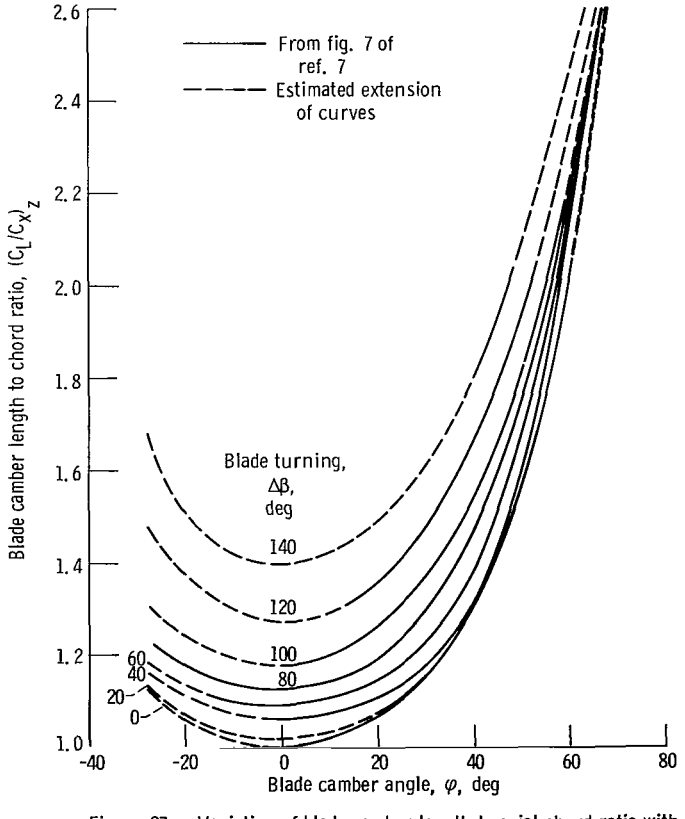

Figure 27. - Variation of blade camber length to axial chord ratio with blade camber angle and blade turning.

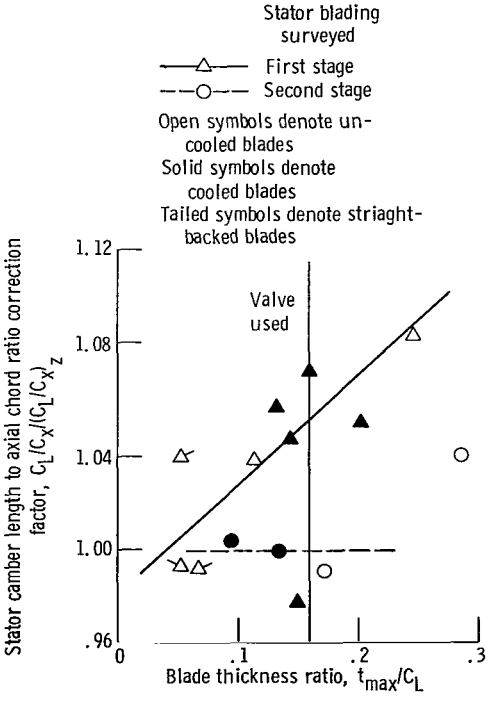

Figure 28. - Variation of correction factor for stator camber length to axial chord ratio with blade thickness ratio.

proximately a linear relation between t_{max}/C_L and the correction factor, and this relation is noted by the solid line drawn on the figure.

Figure 28 also shows that a value of blade thickness parameter t_{max}/C_L of 0.16 was assumed and used for the blading developed in this report. Therefore, for the first-stage stator, this assumption resulted in a correction of plus 6 percent for the values of $(C_L/C_x)_z$ determined in figure 27. The points for the second-stage stator blading surveyed are also shown in figure 28, indicating that no correction in $(C_L/C_x)_z$ was necessary.

Corresponding values for the first- and second-stage rotor blading surveyed are not shown. No definite trends were noted because of a wide scattering of the data for first-stage rotors and a lack of sufficient data for second-stage rotors. Therefore, no correction was made. It was noted, however, that the error in making this assumption could have been as high as ±5 percent in the ratio $(C_L/C_x)/(C_L/C_x)_z$.

Blade surface areas $A_{S,b}$ axial solidity σ_x, number of blades n, and hub and tip wall areas A_w were then computed. It was noted that the survey blading had airfoil perimeter lengths of approximately 2.03 times their mean camber lengths C_L at a value of t_{max}/C_L of 0.16. Therefore, blade surface areas $A_{S,b}$ were computed for each blade row from the following equation:

$$A_{S,b} = 2.03\, C_L \overline{BH} n \tag{21}$$

where $\overline{BH}$ is the blade height at mid-chord and n is the number of blades in each row. Blade number was computed from the equation

$$n = \frac{2\pi r_m}{s} = \frac{2\pi r_m \sigma_x}{C_x} \tag{22}$$

where σ_x is the axial solidity of the blading given in terms of blade entering and leaving angle, and the aerodynamic loading coefficient given in equation (14a) (corrected) of reference 7

$$\sigma_x = \frac{C_x}{s} = \frac{2 \sin \beta_2 \sin(\beta_1 - \beta_2)}{\psi \sin \beta_1} \tag{23}$$

Therefore, equation (21) becomes

$$A_{S,b} = 4.06\ \pi r_m \overline{BH} \sigma_x \left(\frac{C_L}{C_x}\right) \tag{24}$$

The hub and tip wall area per row A_w was assumed to equal twice the mean circumference of the blade row times the axial chord of the blading

$$A_w = 4\pi r_m C_x \tag{25}$$

In so doing, it was assumed that the portion of the wall area in-between blade rows requiring cooling was equal to the portion of the wall area covered by the blades.

APPENDIX F

TURBINE BLADE COOLING

Blade cooling airflow requirements were determined by using the simplified approach of reference 8 for convection cooling. The method consists of making a heat balance between the heat sink required to cool each blade row, to the heat-sink capacity available in the cooling air. The method for predicting the cooling airflow requirements only requires knowledge of the average gas condition in each blade row, the average gas and metal temperatures at the mean radius of the blades, the cooling air supply temperatures, and the thermal cooling effectiveness of the blade cooling design. The following sections summarize the method and the range of the above variables utilized.

Heat-Sink Requirements

The determination of the heat-sink requirements for cooling each row of turbine blading first made use of the following equation:

$$Q_R = \bar{h}_g A_{S,b}(\bar{T}''_g - \bar{T}_M) \tag{26}$$

However, to present the data using a more meaningful reference metal temperature than the average for the entire blade $\bar{T}_M$, the temperature at the mean radius of the blade $T_{M,m}$ was used. The mean radius location was selected because it generally is the structurally critical region of the blade. Along with this change in reference metal temperature, typical average gas temperature profiles were assumed, such as that noted in reference 9. (A schematic of the assumed temperature profiles and notation used in this section and in appendix G is shown in fig. 29.) The profiles assumed were such that the

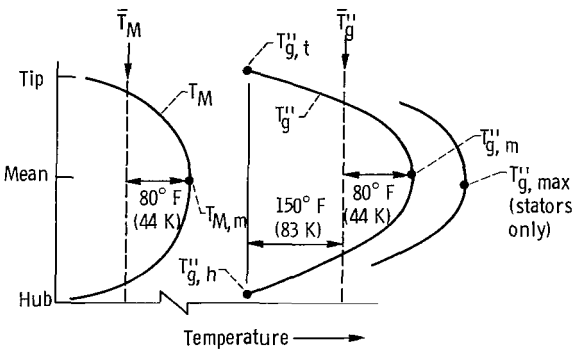

Figure 29. - Typical gas and metal temperature profiles and notation.

gas total temperature relative to each blade row at the mean radius $T''_{g,m}$, was 80° F (44 K) higher than the respective average gas total temperature $\overline{T}''_g$. The average gas total temperature was determined as described in appendixes D and H. Another assumption made was that the gas and blade metal temperature profiles from hub to tip were such that the difference between the gas and the blade metal temperature at the mean radius $(T''_g - T_M)_m$ was equal to the difference between the average gas and blade metal temperature $(\overline{T}''_g - \overline{T}_M)$. This assumption then transforms equation (26) into

$$Q_R = \bar{h}_g A_{S,b}(T''_g - T_M)_m \tag{27}$$

The total surface area of each blade row $A_{S,b}$ was determined as described in appendix E. The average gas-to-blade heat-transfer coefficient for each blade row $\bar{h}_g$ was determined by using the following equation from reference 10:

$$\bar{h}_g = \frac{0.037\ Re_g^{0.8}(Pr_g)^{1/3}k_g}{C_L} \tag{28}$$

where

$$Re_g = \frac{(\overline{\rho_g V_g})C_L}{\mu_g} \tag{29}$$

The term C_L is the average surface distance from the leading edge to the trailing edge, as determined in appendix E. The term $\overline{\rho_g V_g}$ is the arithmetic average of the values of the term at the inlet and outlet of each blade row. The values of the term were obtained from the gas temperatures, pressures, and critical velocity ratios computed in appendix D, and includes the mass-averaging effect of the blade cooling air on ρ_g, as described in appendix H.

The values of the transport properties, Pr_g, K_g, and μ_g in equations (28) and (29) were based on the average total relative temperature of the gas entering the blade row. The range of values of transport properties used are noted in table VI. Alternate approaches were also considered and compared, wherein the transport properties required for equations (28) and (29) were determined from either the average static temperature of the gas entering and leaving each blade row, or from the blade film temperature which was the arithmetic average of the allowable blade metal temperature and the average static temperature of the gas entering and leaving the blade row. In the latter case, film density was also used in place of gas density in equation (28).

TABLE VI. - TURBINE GAS TRANSPORT PROPERTIES

Gas temperature, T_g		Absolute dynamic viscosity, μ		Prandtl number, Pr	Thermal conductivity, k	
^{o}F	K	lb/(ft)(sec)	g/(cm)(sec)		Btu/(sec)(ft)(^{o}F)	J/(sec)(cm)(K)
1200	922	26.3×10^{-6}	391.3×10^{-6}	0.709	10.7×10^{-6}	666×10^{-6}
1800	1255	32.0	476.3	.705	13.8	859
2400	1589	37.3	555.0	.702	17.0	1059
3000	1921	42.3	629.6	.693	20.5	1276

The allowable mean-radius metal temperatures $T_{M,m}$ used in equation (27) were 1800^{o} F (1255 K) for stator blading and 1700^{o} F (1200 K) for rotor blading. It was assumed that these temperatures would provide a 1000-hour life for turbine blading made of currently available high-temperature alloys. The basis for this assumption is discussed in reference 9. These mean-radius blade metal temperatures correspond to average blade metal temperatures $\overline{T}_M$ of 1720^{o} and 1620^{o} F (1211 and 1155 K), respectively, for the stator and rotor blading.

With all the terms on the right side of equation (27) known, the heat sink required to cool each blade row to an allowable mean-radius metal temperature can be determined. The equation with the terms used applies to an engine where essentially no circumferential variation in gas temperature exists, and the mean-radius gas temperature $T''_{g,m}$ is considered to be the critical reference temperature. In actual hot turbine operation, however, the first-stage stator, and to a lesser extent the second-stage stator, is exposed to circumferential gradients in gas temperature (referred to as hot spots) that are considerably hotter than the average gas temperature at the mean radius. To account for this effect in the analysis, a modification was made to equation (26), as suggested in reference 8. The modification made was to multiply the heat-sink requirements as determined by equation (27) for the first-stage stator by the ratio $(T''_{g,max} - T_{M,m})/(T''_g - T_M)_m$. This factor is the ratio of the difference between the hot-spot gas temperature $T''_{g,max}$ and the desired metal temperature $T_{M,m}$ at the mean radius, to the temperature difference in equation (27).

The maximum hot-spot gas temperature ahead of the first-stage stators was determined from the following equation:

$$T''_{g,max} = \overline{T}''_g + PF(\overline{T}''_g - T'_{B,1}) \tag{30}$$

A pattern factor PF of 0.15 was assumed. The maximum hot-spot gas temperature ahead of the second-stage stators was determined by assuming that half of the increase

in gas temperature in the first-stage stator due to the effect of pattern factor was attenuated across the first stage before entering the second stage, so that

$$T''_{g,\,max,\,III} = \overline{T}''_{g,\,III} + \left(\frac{T''_{g,\,max} - \overline{T}''_{g}}{2}\right)_{T,\,1} \tag{31}$$

The heat-sink capacities computed by this method provide for cooling to the allowable metal temperature of only the stator blading in the circumferential location exposed to the hot spot, and over-cool the remaining stator blades.

Heat-Sink Capacity Available

The heat-sink capacity in the compressor bleed air available for cooling the blading was obtained from the equation

$$Q_A = \left[(w\overline{C}_P)(T''_2 - T''_1)\right]_{y,\,b} \tag{32}$$

For the purpose of the analysis, this equation was modified to include the following:

(1) The thermal cooling effectiveness of the blade cooling configuration

$$\Lambda = \frac{(T''_2 - T''_1)_{y,\,b}}{(\overline{T}_M - T''_{y,\,b,\,1})} \tag{33}$$

(2) The effect of the difference between the average metal temperatures at the mean radius and the average for the entire blade $(T_{M,\,m} - \overline{T}_M)$, which was assumed to be 80° F (44 K) to be compatible with the difference between the average and mean-radius gas temperatures assumed $(T''_{g,\,m} - \overline{T}''_{g})$

(3) The ratio of the compressor exit bleed flow used for cooling the blading to the flow entering the compressor $w_{y,\,b}/w_e$. With these modifications incorporated, equation (32) becomes

$$Q_A = \left(\frac{w_{y,\,b}}{w_e}\right) w_e (\overline{C}_{P,\,y}) \Lambda \left[T_{M,\,m} - (T''_{y,\,b,\,1} + 80^{\circ}\text{ F})\right] \tag{34}$$

Values of blade thermal cooling effectiveness Λ of 0.5, 0.6, and 0.7 were as-

sumed. As indicated in reference 8, the first value of 0.50 represents that attainable with currently available convection-cooled configurations, and the third value of 0.70 represents an advanced convection-cooling design. The temperature of the air supplied to the blades $T''_{y,b,1}$ was assumed to be constant to all blade rows, and was assumed to range from that of the compressor discharge temperature of the engines analyzed to a temperature 600° F (333 K) lower. Current practice is to use air at compressor discharge temperature ($\Delta T'_{HX,y} = 0$). However, a reduction in compressor discharge temperature of up to 600° F (333 K) was assumed to be attainable with the heat-exchanger system noted in figure 3, either by itself or in combination with the various heat-sink systems described in reference 3. The value of specific heat used in equation (34) was evaluated at the arithmetic average of the cooling air inlet and exit temperatures from the blading.

Thus, for a given compressor inlet air flow, blade thermal cooling effectiveness, cooling air temperature, and allowable mean-radius blade metal temperature, the heat-sink capacity available in the compressor bleed air was determined from equation (34). The relation between this heat-sink capacity available to that required (eq. (27)) provided the required coolant airflow ratio y_b for each turbine blade row

$$y_b = \left(\frac{w_{y,b}}{w_e}\right) = \frac{\bar{h}_g A_{S,b}(T''_g - T_M)_m}{w_e \bar{C}_{P,y} \Lambda \left[T_{M,m} - (T''_{y,b,1} + 80^\circ \text{ F})\right]} \tag{35}$$

APPENDIX G

TURBINE HUB AND TIP WALL COOLING

In addition to determining the cooling airflow requirements for the airfoil portion of the stator and rotor blading, the airflow required to cool the blade hub platforms and turbine shroud and tip walls (herein referred to as hub and tip walls) was determined. The calculations to determine the airflow required several simplifying assumptions to avoid problems associated with the details of the geometry of the cooling scheme. It was first assumed that the walls would be film-cooled. The film-cooling correlation used (eq. (36)) was obtained from relations developed in reference 11

$$\frac{T_{M,w,ad} - T_g''}{T_y'' - T_g''} = \frac{1.9(Pr)^{0.67}}{1 + 0.329\left(\frac{C_{P,g}}{C_{P,y}}\right)\left(\frac{\mu_g}{\mu_y}\right)^{0.2}\left(\frac{\rho_g V_g x}{\rho_y V_y B}\right)^{0.8} Re_w^{-0.2}\,\chi} \tag{36}$$

where

$$\chi = 1 + 0.15\times10^{-3}\, Re_w\left(\frac{\mu_y}{\mu_g}\right)\sin\alpha \tag{37}$$

and where

$$Re_w = \frac{\rho_y V_y B}{\mu_y} \tag{38}$$

In order to simplify the analysis, the cooling air was assumed to be injected parallel to the walls. As a result, angle α between the cooling airflow and gas flow in equation (37) was zero, and the value of χ became 1. For this condition, the cooling airflow requirements for film cooling the hub and tip wall region were minimized. Another simplification was the assumption that conduction cooling effects were small so that the hub or tip wall metal temperatures $T_{M,w}$ were equal to the adiabatic wall temperatures $T_{w,ad}$.

By writing the coolant airflow ratio required to cool either the hub or tip wall of each blade row in terms of the coolant slot height B and an effective circumference, an equation for the continuity of flow over the walls was obtained as follows:

$$\left(\frac{w_{y,w}}{w_e}\right)_h = y_{w,h} = \frac{(\rho V)_{y,w} B\left[\pi D_{T,h}(1 - \Delta)\right]}{w_e} \tag{39}$$

where equation (39) was written in terms of the hub wall, but would also apply to the tip wall with proper subscripts. The term in the bracket was the effective circumference of the slot, defined in terms of the hub (or tip) diameter of the blade row, $D_{T,h}$ (or $D_{T,t}$), and the amount of circumference that was not blocked by the blades $1 - \Delta$. For the purpose of this analysis, the blockage term Δ was assumed to have a value of 0.2.

Combining equations (36) and (39) and utilizing the assumptions made resulted in the following equation for the coolant airflow ratio required to cool the hub wall (or tip wall with appropriate subscript changes) for each blade row:

$$y_{w,h} = \frac{0.827}{w_e}\left\{\left(\frac{C_{P,g}}{C_{P,y}}\right)\frac{\mu_g^{0.2}(\overline{\rho_g V_g} x)^{0.8} D_{T,h}}{\left[\frac{1.9(Pr)^{0.67}}{\lambda} - 1\right]}\right\} \tag{40}$$

where

$$\lambda = \frac{T''_{g,h} - T_{M,w}}{T''_{g,h} - T''_y} \tag{41}$$

To further simplify the analysis herein, it was assumed that the conditions at the hub and tip were the same for any given blade row. The gas temperature T''_g at the hub and tip was assumed to be 150° F (83 K) less than the average gas relative total temperature $\overline{T}''_g$ computed in appendixes D and H. This assumption is illustrated in figure 29 and is based on a typical radial gas profile used in reference 9. Assuming the same relative gas temperature for the hub and tip walls of the rotor row implies a shrouded turbine. The allowable metal temperature of the hub and tip walls $T_{M,w}$ was assumed to be 1600° F (1140 K). The cooling air temperature T''_y was at either the compressor exit temperature $T'_{C,2}$ as noted in table I, or at a lower value to represent cooling of the compressor bleed air by means of the fuel-to-air heat exchanger shown in figure 3, or by other means as described in reference 3.

The values of the specific heat capacity $C_{P,g}$ and viscosity μ_g were determined at the wall gas temperature $T''_{g,h}$ or $T''_{g,t}$ for each blade row. The specific heat capacity of the cooling air $C_{P,y}$ was determined at temperature T''_y. The Prandtl number Pr was evaluated at the arithmetic average between the hub and tip wall gas temperature, and the temperature of the cooling air T''_y. The term $\overline{\rho_g V_g}$ was assumed to

be the arithmetic average of the inlet and exit values at the mean radius for each blade row. The radial variation of the term from hub to tip was approximately linear and the variation was not large. The effective distance traveled by the cooling air film through the row x was assumed to be equal to the mean camber length C_L of the blade times a factor of 1.2 to account for an extension of the walls beyond the leading and trailing edge of the blading. Utilizing these assumptions, the coolant airflow ratio required to cool both the hub and tip walls of each blade row was determined by the resulting equation

$$y_w = \frac{\frac{1.914}{w_e}\left(\frac{C_{P,g}}{C_{P,y}}\right)\mu^{0.2}(\overline{\rho_g V_g} C_L)^{0.8} D_{T,m}}{\frac{1.9\ Pr^{0.67}}{\bar{\lambda}} - 1} \tag{42}$$

where

$$\bar{\lambda} = \frac{1600^{\circ}\ F - (\overline{T}''_g - 150^{\circ}\ F)}{T'_y - (\overline{T}''_g - 150^{\circ}\ F)} \tag{43}$$

The sum of the coolant airflow ratios for each row, as obtained from equation (42), provided the total coolant airflow ratio required to cool the walls of the entire turbine.

APPENDIX H

CALCULATION PROCEDURE

An iterative calculation was required to incorporate the assumptions of appendixes C to G into the design of the turbines. Because of the iterative procedure, the term "base" turbine was used to define the initial assumptions and designs resulting from the first iteration. First, a base turbine design was computed for each engine where the following steps were taken:

(1) The cooling airflow ratios noted in table I were used to compute the specific work (eq. (14)) at cruise, and the associated velocity diagrams (hub, mean, and tip) for each turbine.

(2) The weight flow at takeoff for each turbine was assumed to be equal to the burner discharge flow plus one-half of the blade cooling airflow, and to be held constant across the turbine

$$w_{T,1} = w_{T,2} = w_{B,2} + \left(\frac{w_{y,b}}{2}\right) \tag{44}$$

In so doing, it was also assumed that the turbine inlet temperature was not reduced by the addition of the cooling air $T'_{T,1} = T'_{B,2}$. A schematic of the flow model used for this "base" turbine design is shown in figure 30(a).

Step (2) resulted in the "base" turbines having first-stage stator and second-stage rotor blade heights slightly longer and shorter, respectively, than an actual cooled turbine would have because in an actual design, entry of the cooling air would be distributed between the four blade rows.

Next, the cooling airflow ratios were computed at engine cruise conditions for each blade row of the "base" turbine designs, and the following adjustments were made to the inner-stage gas stream temperatures and blade heights:

(3) The relative total temperature of the blade cooling air and gas flow entering each blade row was adiabatically mixed (weight averaged) to obtain an after-mixed relative total gas temperature leaving the blade row

$$(T''_g)_{b,2} = \frac{(wT'')_{g,b,1} + (wT'')_{y,b,1}}{(w_g)_{b,2}} \tag{45}$$

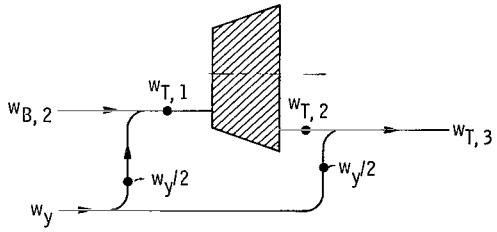

(a) Model used to determine "base" design of turbine.

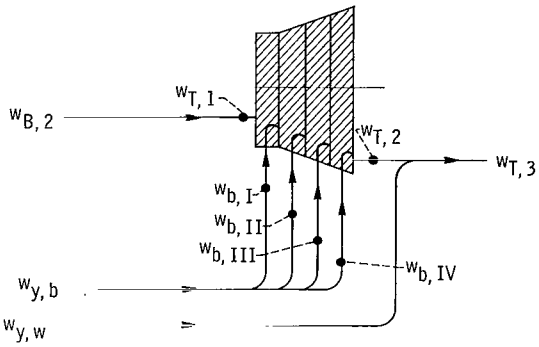

(b) Model used to determine blade cooling air effects on inner-stage gas temperatures.

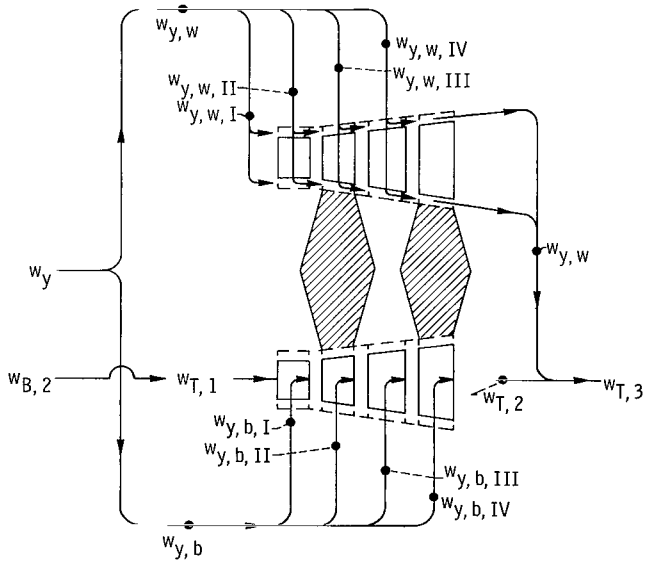

(c) Model used to incorporate wall cooling air to design of turbine.

Figure 30. - Turbine flow models.

where

$$(w_g)_{b,2} = (w_g)_{b,1} + (w_y)_b \tag{46}$$

As noted previously, the relative total temperature of the cooling air available to the rotor blading $T''_{y,r}$ was assumed to be equal to the absolute total temperature of the cooling air available to the stator blades $T''_{y,s}$. Figure 30(b) shows schematically the flow model used for step (3).

(4) The blade height of each row was adjusted to accommodate the new after-mixed condition of the gas and blade cooling air leaving the preceding blade row. The subscripting in the equation for this assumption varied with blade row. For the second-stage stator (third blade row) the equation was

$$(BH)_{III,j+1} = (BH)_{III,j}\left(\frac{w_{j+1}}{w_j}\right)_{II,2}\left(\frac{\bar{\rho}_j}{\bar{\rho}_{j+1}}\right)_{III} \tag{47}$$

Steps (3) and (4) were repeated until succeeding iterations converged on a correct combination of blade cooling airflow ratio, inner-stage gas temperature, and blade height for each blade row of the "base" turbine designs. Wall cooling airflow ratios $w_{y,w}/w_e$ were then computed (eq. (42)) and added to the blade cooling airflow ratio $w_{y,b}/w_e$, giving the total cooling airflow ratio required for each turbine

$$y = \left(\frac{w_y}{w_e}\right) = \frac{w_{y,w} + w_{y,b}}{w_e} \tag{48}$$

The cooling airflow ratios used in step (1) were then replaced with the computed ratio for each design (eq. (48)), and the entire calculation procedure was repeated until successive calculations produced repeating values of the cooling airflow ratio.

All flow velocities, angles, and blade mean diameters computed in the preceding procedure for the "base" turbine designs (steps (1) and (2)) were assumed to be fixed during the iterative calculations of steps (3) and (4) to assure no change in turbine specific work. The critical velocity ratio of the gas flow increased as it expanded through the turbine because of the inclusion of the blade cooling air (step (3)), and the effect that this cooling air had on reducing the temperature and critical velocity of the gas at the exit of each blade row. The design exit critical velocity ratios of approximately 0.45 and 0.50, assumed for the turbines of the afterburning and dry turbojet engines, respectively, included this effect.

A final adjustment of blade height was required to accommodate the hub and tip wall cooling airflow, and this adjustment was computed from the following continuity equation:

$$\frac{(A_a)_{y,w}}{(A_a)_{g+y,b}} = \frac{(\Delta BH)_{y,w}}{(BH)_{g+y,b}} = \frac{\left(\frac{w}{\rho V_x}\right)_{y,w}}{\left(\frac{w}{\rho V_x}\right)_{g,m+y,b,m}} \tag{49}$$

In incorporating the wall cooling air into the calculation procedure, the following assumptions were made:

(5) In equation (49),

$$(V_x)_{y,w} = \frac{(V_x)_{g,m}}{2} \tag{50}$$

$$(\rho)_{y,w} = \left(\frac{p}{RT}\right)_{y,w} = \frac{(p)_{g,m}}{(RT)_{y,w}} \tag{51}$$

and, for any blade row,

$$w_{y,w} = w_{y,w,I} + w_{y,w,II} + \cdots \tag{52}$$

(6) The wall cooling air did not mix with the main gas stream or contribute to the work output of the turbine.

(7) The additional length of blading necessary to pass the wall cooling air was cooled by this cooling air, and therefore did not require an increase in the blade cooling airflow. The flow model incorporating these final assumptions is shown in figure 30(c).

The turbine exit temperature after mixing with the wall cooling airflow at station 3 (fig. 30(c)) was determined by weight averaging the total wall cooling airflow required for the turbine with the gas flow at station T2.

$$T'_{T,3} = \frac{(T'w)_{T,2} + (T'w)_{y,w}}{w_{T,3}} \tag{53}$$

REFERENCES

1. Whitlow, John B., Jr.; Eisenberg, Joseph D.; and Shovlin, Michael D.: Potential of Liquid-Methane Fuel for Mach-3 Commercial Supersonic Transports. NASA TN D-3471, 1966.

2. Koenig, Robert W.; and Kraft, Gerald A.: Influence of High-Turbine Inlet Temperature Engines in a Methane-Fueled SST when Takeoff Jet Noise Limits are Considered. NASA TN D-4965, 1968.

3. Miller, Brent A.: Analysis of Several Methane-Fueled Engine Cycles for Mach 3.0 Flight. NASA TN D-4699, 1968.

4. Schum, Harold J.; Petrash, Donald A.; and Nunamaker, Robert R.: Experimental Investigation of Two-Stage Air-Cooled Turbine Suitable for Flight at Mach 2.5. NASA TM X-148, 1959.

5. Lueders, H. G.: Experimental Investigation of Advanced Concepts to Increase Turbine Blade Loading. 2: Performance Evaluation of Plain Rotor Blade. NASA CR-1172, 1968.

6. Schum, Harold J.; and Davison, Elmer H.: Component Performance Investigation of J-71 Experimental Turbine. I - Over-all Performance with 97-Percent-Design Stator Areas. NACA RM E54J15, 1956.

7. Zweifel, O.: Optimum Blade Pitch for Turbo-Machines with Special Reference to Blades of Great Curvature. The Engineer's Digest, vol. 7, nos. 11 and 12, Nov. and Dec. 1946.

8. Stepka, Francis S.: Considerations of Turbine Cooling Systems for Mach 3 Flight. NASA TN D-4491, 1968.

9. Burggraf, F.; Murtaugh, J. P.; and Wilton, M. E.: Design and Analysis of Cooled Turbine Blades. Part 1 - Leading and Trailing Edge Configurations. Rep. R68AEG101, General Electric Co. (NASA CR-54513), Jan. 1, 1968.

10. Eckert, E. R. G.: Introduction to the Transfer of Heat and Mass. McGraw-Hill Book Co., Inc., 1950.

11. Goldstein, R. J.; and Haji-Sheikh, A.: Prediction of Film Cooling Effectiveness. Paper No. 225 presented at the Japan Soc. Mech. Eng., 1967 Semi-International Symposium, Tokyo, Japan, Sept. 4-8, 1967.

NASA-Langley, 1970 — 28 E-5602

"The aeronautical and space activities of the United States shall be conducted so as to contribute . . . to the expansion of human knowledge of phenomena in the atmosphere and space. The Administration shall provide for the widest practicable and appropriate dissemination of information concerning its activities and the results thereof."

—NATIONAL AERONAUTICS AND SPACE ACT OF 1958

NASA SCIENTIFIC AND TECHNICAL PUBLICATIONS

TECHNICAL REPORTS: Scientific and technical information considered important, complete, and a lasting contribution to existing knowledge.

TECHNICAL NOTES: Information less broad in scope but nevertheless of importance as a contribution to existing knowledge.

TECHNICAL MEMORANDUMS: Information receiving limited distribution because of preliminary data, security classification, or other reasons.

CONTRACTOR REPORTS: Scientific and technical information generated under a NASA contract or grant and considered an important contribution to existing knowledge.

TECHNICAL TRANSLATIONS: Information published in a foreign language considered to merit NASA distribution in English.

SPECIAL PUBLICATIONS: Information derived from or of value to NASA activities. Publications include conference proceedings, monographs, data compilations, handbooks, sourcebooks, and special bibliographies.

TECHNOLOGY UTILIZATION PUBLICATIONS: Information on technology used by NASA that may be of particular interest in commercial and other non-aerospace applications. Publications include Tech Briefs, Technology Utilization Reports and Notes, and Technology Surveys.

Details on the availability of these publications may be obtained from:

SCIENTIFIC AND TECHNICAL INFORMATION DIVISION

NATIONAL AERONAUTICS AND SPACE ADMINISTRATION

Washington, D.C. 20546